

# A Tutorial on Learning Disentangled Representations in the Imaging Domain

Xiao Liu\*, Pedro Sanchez\*, Spyridon Thermos, Alison Q. O’Neil and Sotirios A. Tsaftaris, *Senior Member, IEEE*,

**Abstract**—Disentangled representation learning has been proposed as an approach to learning general representations. This can be done in the absence of, or with limited, annotations. A good general representation can be readily fine-tuned for new target tasks using modest amounts of data, or even be used directly in unseen domains achieving remarkable performance in the corresponding task. This alleviation of the data and annotation requirements offers tantalising prospects for tractable and affordable applications in computer vision and healthcare. Finally, disentangled representations can offer model explainability and can help us understand the underlying causal relations of the factors of variation, increasing their suitability for real-world deployment. In this tutorial paper, we will offer an overview of the disentangled representation learning, its building blocks and criteria, and discuss applications in computer vision and medical imaging. We conclude our tutorial by presenting the identified opportunities for the integration of recent machine learning advances into disentanglement, as well as the remaining challenges.

**Index Terms**—disentanglement, disentangled representation, content-style, applications, tutorial, computer vision, medical imaging.

## 1 INTRODUCTION

IMAGINE that you want to endow an autonomous driving car with an optical system that can localise and detect road signs. This system must be robust to light changes, sensor noise and distortions, occlusions, and variations of the sign. Alternatively, imagine a system that localises the heart in Magnetic Resonance Imaging (MRI) and Computerised Tomography (CT) scans. This system needs to be robust to any changes in imaging process, scanner, noise, as well as anatomical and pathological variation. Regardless of the application domain, the current deep (supervised) learning paradigm indicates that we *must* present to the system as many examples as possible to make it robust and learn what is unnecessary, or nuisance [1], *e.g.* the angle between the camera and sign or the patient being placed rotated in the scanner, as opposed to what matters, *i.e.* the location of the sign or of the heart. But in reality, collecting and annotating enough data to cover the real-world variation is an extremely time-consuming and costly solution, hence not realistic. On the other hand, algorithms trained on existing annotated data exhibit drastic performance reduction when deployed in the real-world settings due to the data distribution shift [2, 3, 4].

Surprisingly, we may not always need annotated data or –carefully crafted– data augmentations to achieve this. With disentangled representation learning (DRL), one learns to encode the underlying factors of variation into separate latent variables [5, 6], which ultimately capture sensitive and useful information for the task at hand and also understand

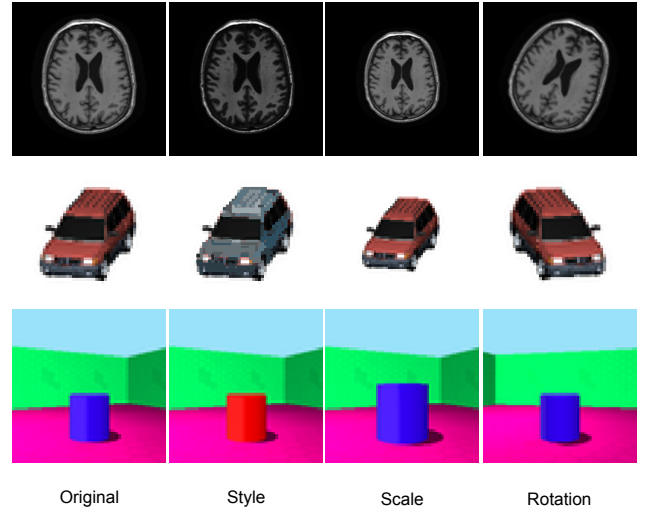


Fig. 1. Examples of factors of variations: style, scale, and rotation in the context of brain scans [7], cars [8], and 3D shapes [9].

the underlying causal relations amongst the variables. We choose to introduce the reader to DRL by presenting 3 indicative examples of disentangled factors in Fig. 1, which affect the colour, scale, and rotation of the rendered object in the corresponding scene. By adopting DRL, one can design deep models that will be robust to representations from unseen domains, a result that cannot be always achieved through data augmentation.

In this paper<sup>1</sup>, we want to consolidate understanding of

- \*Authors contributed equally
- X. Liu, P. Sanchez, S. Thermos, and S.A. Tsaftaris are with the School of Engineering, The University of Edinburgh, Edinburgh, UK. S.A. Tsaftaris is also with the The Alan Turing Institute, London, UK  
E-mail: {Xiao.Liu, Pedro.Sanchez, SThermos, S.Tsaftaris}@ed.ac.uk
- A.Q. O’Neil is with Canon Medical Research Europe and with the School of Engineering, The University of Edinburgh, Edinburgh, UK  
E-mail: alison.oneil@mre.medical.canon

1. This paper follows a tutorial style, but also surveys a considerable (200 citations) number of works. It aims to be concise and not fully survey the field (only in 2021, 1700 papers on arXiv on disentangled in machine learning have appeared). It originates from two tutorials in MICCAI on disentangled representations <https://vios.science/tutorials/dream2021> and benefits greatly from feedback received from the audience of these tutorials.

representation learning and disentanglement and applications in computer vision and medical imaging. Our goal as **learning objectives** for the reader are to:

- 1) Understand what is a representation space and why (in)variance matters.
- 2) Understand the impact of causal relations in the context of disentangled representations.
- 3) See the need for disentanglement through the lens of limited observations.
- 4) Understand that disentanglement requires at least one of: inductive biases, priors, or supervision.
- 5) Learn basic building blocks for encouraging disentanglement.
- 6) Explore computer vision and healthcare applications.
- 7) Identify opportunities emerging from combining disentanglement with new concepts, tasks, and learning techniques, and the existing challenges.

To define disentanglement we first offer theory and fundamentals of machine learning and learning representations. We then provide an overview of key generative models that constitute the basis of many subsequent models, as well as the building blocks of disentanglement and the metrics used to evaluate it. We discuss key models designed to address applications of disentanglement in the vision and medical imaging domains follows. We conclude discussing opportunities and challenges.

## 2 THEORY AND FUNDAMENTALS: CONCEPTS OF REPRESENTATION LEARNING

**Notation.** Here, we define notation used throughout the paper. In particular, we use  $x$ ,  $\mathbf{x}$  and  $X$  to denote scalars, vectors, and higher-dimensional tensors drawn from a respective dimensional domain  $\mathcal{X}$ . We use  $X_i$  to refer to a datum of the above tensors (of any dimension) for presentation simplicity where the dimensionality of the tensor is assumed to be understood by the context. Additionally, we assume we have access to a dataset containing samples of  $X_i$ , where  $i \in [1, N]$ ,  $N$  denoting the number of samples. We use  $\mathcal{X}$  to denote the observed variables of the input domain,  $\mathcal{Z}$  for latent representations,  $\mathcal{S}$  for real generating factors, and  $\mathcal{Y}$  for the output domain. For example, if we choose to solve a classification task, then  $\mathcal{Y}$  is a space of scalars  $y$ .

### 2.1 Model learning

Learning a model is defined as the task of learning a mapping between the two domains [10], i.e.  $f : \mathcal{X} \rightarrow \mathcal{Y}$ . It usually relies on the –somewhat strong– assumption that the input data is *independent and identically distributed* (i.i.d).

While  $f$  can be anything, for the purpose of this article we will assume a *compositional* view to model learning. In other words  $f$  can be split into to components, namely  $f : E_\phi \circ D_\theta$ . The goal of  $E_\phi$  is to achieve the mapping  $E_\phi : \mathcal{X} \rightarrow \mathcal{Z}$ , where  $\mathcal{Z}$  is an intermediate latent representation and  $D_\theta$  achieves the mapping  $D_\theta : \mathcal{Z} \rightarrow \mathcal{Y}$ . We will call  $E_\phi$  as “encoder” and  $D_\theta$  as “decoder”.<sup>2</sup> Thus, the role of the encoder is to arrive at an appropriate latent representation

for the task, whereas the role of the decoder is to transform this representation into the domain of the output task.

To learn and optimise the parameters  $\phi$  and  $\theta$ , an appropriate training objective  $\ell$  is necessary. The functions  $E_\phi$  and  $D_\theta$  can be approximated with deep –some say over-parametrised– neural networks, which have recently seen considerable success due to their expressiveness and abilities to approximate highly non-linear mappings [11]. Thus, the goal of model learning is the solution of the task at hand through learning a good representation. We present in the next section desirable properties of a good representation.

### 2.2 Representation learning

The task of finding a good representation for the task at hand is fundamental in machine learning, with even a dedicated conference, namely the *Internal Conference on Learning Representations* (ICLR, <http://iclr.cc>). While landmark reviews exist [2, 5], herein we use an autonomous driving example to pose key questions. Consider a task of detecting cars. The scene may have a car of different colour, make and brand, as well as different backgrounds, such as buildings, people, road surface, etc. The task then is to put a bounding box  $y_i$  around each car in the image ( $X_i$ ). We then consider the following questions: *What properties would we like the learned representation  $\mathcal{Z}$  to have?*

Clearly, if the car changes location in the image, we would like the bounding box output to change location accordingly. In other words, we would like our representation to be *equivariant* to the location of the object. On the other hand, we would like the output to remain the same if the colour of the car changes. Our representation should thus be *invariant* to colour-related changes, whether locally in the object or globally in the scene. To put these concepts in mathematical terms, let us define a group of symmetries  $\Omega$ . Symmetries are *transformations* that leave some aspects of the input intact [12, 13, 14]. For instance, the category of an object does not change applying shift operations on the image, therefore these operations are considered symmetries in the object recognition domain. Using the model  $f$  and symmetries  $\Omega$ , we now proceed to define the equivariance and invariance properties.

**Equivariance.** A function  $E_\phi : \mathcal{X} \rightarrow \mathcal{Z}$  is equivariant w.r.t.  $\Omega$ , if there is a transformation  $\omega \in \Omega$  of the input  $X \in \mathcal{X}$  that affects the output  $Z \in \mathcal{Z}$  in the same manner. Formally, this means that  $\Omega$ -equivariance of  $E_\phi$  is obtained when there exists a mapping  $M_\omega : R^d \rightarrow R^d$  applying  $\omega$  to an input such that:

$$E_\phi(M_\omega \circ X) = M_\omega \circ E_\phi(X), \forall \omega \in \Omega. \quad (1)$$

In practice, one chooses transformations that induce the desired equivariance and learned properties in accordance with the task at hand, and thus require a good understanding of the problem (also known as *domain knowledge*) [15]. Other classical examples where equivariance to translation, shift, and mirroring might be important, are tasks such as image segmentation, pose estimation, and landmark detection. In these cases, the goal is for the output to change exactly as the input upon applying any of these geometric transformations.

<sup>2</sup>  $D_\theta$  is often referred as a classifier or a regressor, however we avoid this nomenclature here, to be more general.

**Invariance.** A special case of equivariance occurs when  $M_g$  becomes the identity map. Formally,  $E_\phi$  is invariant to transformations of  $\Omega$  if:

$$E_\phi(M_\omega \circ X) = E_\phi(X), \forall \omega \in \Omega. \quad (2)$$

With the aforementioned formal definitions, it becomes evident that we need to define the set of transformations  $\omega$  to which we want our model to be invariant (e.g. a change of intensity) or equivariant (e.g. object translation). Naturally, one then asks: *How are these sets of transforms defined? How is the desired invariance or equivariance of  $\mathcal{Z}$  enforced?* The transforms are usually task-specific, we show how each model introduces different biases to approximate the transformations in section 6.

### 2.3 Generating factors

Considering a distribution that characterises the domain  $\mathcal{X}$ , the *generating factors*  $\mathcal{S}$  are the underlying variables that fully characterise the variation of the data - seen or expected to be seen. Recent studies [2, 5] argue that representations should enable the decomposition (i.e. disentanglement) of the input data into separate factors. Each factor should correspond to a variable of interest in the underlying process that generated the data. For the rest of the paper we will refer to the real-world generating factors as “real” and to the ones learned by a model as “learned”.

Considering the autonomous driving example, we can think of several variables: car colour, car shape, car location, sun location, light intensity, texture of the road, etc. In fact, the more complex the scene the more complex the variables, and the higher the number of possible combinations. In fact, as Yuille and Liu [16] report, enumerating the combinations of generating factors readily arrives at an explosion of the possible combinations that a dataset must contain to enable a model learn the desired in/equi-variances.

Of course, it is not realistic to identify every factor and cover every possible combination. This is where domain knowledge becomes valuable. It is domain knowledge that enables the elucidation of as many factors as possible and allows us to define which real factors we want to be in/equi-variant to. For example, if a model performs poorly in a subset of a dataset, e.g. yellow cars, one could explicitly force the model to learn a representation invariant to colour changes, thus improving the model’s generalisation ability.

### 2.4 A causal perspective

One can readily appreciate that the real factors are not the same as those learned from the available data. In fact, it is our objective to learn representations that simulate the real factors as accurately as possible. Learning good representations of the real factors, however, might not be enough, since these factors are not truly independent from each other. In reality, they are connected via causal relations. For example, the presence of a car causes the presence of wheels, tyres, etc. Causal relations are directional: the effect will change given an *intervention* (change) on the cause, but not the other way around. Therefore, representation learning can also be seen from the lens of causal inference [2].

The mathematical formalism around causality pioneered by Pearl *et al.* [4] presents a different domain knowledge-driven perspective on representation learning. It is a framework where one can model the data generation process and include assumptions about a given problem. The so-called *do-calculus* allows sampling from an interventional distribution entailed by a Structural Causal Model (SCM). SCMs consist of graphs where the nodes are generating factors and the edges are causal relationships [3]. In fact, these edges represent physical mechanisms of the real world. As reported in Sec. 2.5, understanding these relations is a critical step towards learning robust representations.

The notion of *causality* goes beyond statistical tools for learning representations, towards analysing how a system would react upon an intervention. This is known as Pearl’s causal hierarchy [4, 17]. With SCMs, one might also answer *counterfactual* queries, such as “what would have happened to an individual if variable ‘ $S_i$ ’ had been different?”. This can be seen as an intervention at individual level. These tools are useful not only for quantifying causal effects, but also to encourage the representation of generating factors to be disentangled (we define disentanglement in Sec. 2.6) as shown by Caselles *et al.* [18] and Besserve *et al.* [19].

### 2.5 Domain shifts

As reported in Sec. 2.1, the i.i.d. is a strong assumption; all datasets are somehow biased due to the finite nature of the acquired data. The hidden generating factors might influence the variables of interest in ways that might decrease algorithmic performance. Following the autonomous driving example presented earlier, a car can be a convertible, but we know that convertibles are not common in Alaska so the “weather” and “geographical location” factors are implicitly related to the car “shape” variable.

Therefore, understanding the data generating process and the underlying causal relations can help to distill the important visual information, and to create mechanisms that are more generalisable. This type of reasoning enables the design of principled strategies for mitigating the data bias [20]. In fact, we can explicitly define which changes we want our model to be invariant or equivariant to, by modeling domain shifts such as: (i) population, i.e. different cohorts, (ii) acquisition, i.e. different cameras, sites or scanners, and (iii) annotations shift, i.e. different annotators.

In the following section, we discuss the disentangled representation learning paradigm, as a promising solution for the challenges described until now. It should improve the learned representation with equi/in-variances to specific undesired variables, taking into account the data generation process and potential domain shifts.

### 2.6 Disentangled representations

Although a widely accepted definition of disentangled representations is yet to be defined, the main intuition is that by disentangling, we separate out the main factors of variation that are present in our data distribution [5, 6, 18, 21]. We characterise a factor as “disentangled” when any intervention on this factor results in a specific change in the generated data [18, 22].

### 2.6.1 Formalising disentanglement

Higgins *et al.* [6] have recently presented a generic definition for disentanglement. Given a compositional world  $W$  and a set of transformations  $\Omega$  (as defined in Sec. 2.2), they define a function  $f : W \rightarrow Z$  that can induce  $\Omega$  in the latent representation  $Z \in \mathcal{Z}$  in an equivariant manner. The representation  $Z$  is defined as “disentangled” if there is a decomposition  $Z = Z_1 \times \dots \times Z_n$  such that a transformation  $\omega$  applied on  $Z_i$  will result in an equivalent transformation in the input domain  $\mathcal{X}$ , leaving all other aspects controlled by  $Z_{j \neq i}$  unchanged. This definition meets the desired properties of a disentangled representation as defined by several works in DRL [5, 23, 24, 25]: a) modularity, *i.e.* each latent dimension should encode no more than one generative factor, and b) informativeness, *i.e.* all underlying generative factors are encoded in the representation.

A complementary view to Higgins *et al.* definition comes from the Information Bottleneck (IB) principle introduced in [26]. IB allows for learning “good” representations for the task at hand, by trading-off sufficiency and complexity. Adopting IB, Achille and Soatto [1] argue that such representations should be: (i) *sufficient* for the task, meaning that we do not discard information required for the output, (ii) among all sufficient representations, it should be *minimal* retaining as little information about the input as possible, and finally (iii) it should be *invariant* to nuisance effects so that the final classifier will not overfit to any correlations between the dataset nuisances and the ground truth labels.

From a causal perspective, one can consider most recent advances [21, 27, 28, 29] as learning the causal variables (*i.e.* generating factors) of a problem without explicitly modeling the causal mechanisms between them.

### 2.6.2 Identifiability

As shown by Locatello *et al.* [21], learning disentangled representations without any type of supervision is impossible. The authors argue that there exists an infinite family of models that could have generated the observed data. From a causal perspective, it is impossible to infer the causal generative process from observational data alone [3]. In other words, *identifying* the model that generated the data without any additional information is impossible. Given an observation  $X$ , there is an infinite number of deep generative models that could have generated a sample from the same marginal distribution [3, 21, 30].

Another theory that supports the findings of Locatello *et al.* is the non-linear ICA framework presented in [31]. In this work, Hyvärinen *et al.* show that even though the linear ICA is identifiable, the flexibility given by non-linear ICA makes it non-identifiable without extra information. More recent works, such as [30] bridge the gap between non-linear ICA and other deep latent variables models, and show that previous unsupervised disentanglement methods were, indeed, non-identifiable.

### 2.6.3 Disentanglement as Inductive Bias

The solution for the identifiability issue is the use of domain knowledge in the design of our systems, *i.e.* the *inductive bias*, instead of using explicit supervision [3, 21, 30].

Current representation learning already enjoys the benefits of inductive biases through the adoption of Convolutional Neural Networks (CNNs) [32] and Recurrent Neural Networks (RNNs) [33]. CNNs, for example, introduce inductive biases about the local correlation in natural images, since convolutions operate over neighbours of a central pixel or voxel. Additionally, convolutions are translation equivariant, and when combined with pooling can offer translation invariance for certain tasks. Apart from the visual domain, language has been modeled with recurrent neural networks that capture the sequential nature of data for making predictions [34]. Recent attention and self-attention models, such as the transformer architecture [35], focus on learning the internal structure of the the input data. These self-attention models essentially learn the best inductive biases for each sample in the data distribution.

Overall, disentangled representations aim to give structure to the learned representations that correspond to the underlying generation process, thus being a useful bias. It is this bias that makes the utilized models identifiable. One of the goals of this paper is to highlight the various inductive biases as building blocks for disentanglement.

## 3 MODELS THAT ENFORCE DISENTANGLEMENT

We now proceed to review the fundamental model architectures designed to encode and disentangle factors of variation as latent variables. We first present the variational and generative models that enforce disentanglement in a vector latent space. We then introduce more recent trends of disentangling using normalisation flows, as well as content-style disentanglement.

### 3.1 Variational Autoencoders

Standard Auto-Encoders (AEs) or Variational Auto-Encoders (VAEs) [36, 37] decompose classification-related factors through image reconstruction [38, 39]. A typical VAE, depicted in Fig. 2(a), learns a compressed and factorised representation  $\mathbf{z}$  from an input  $X$  in an unsupervised manner. VAEs discover and disentangle the factors of variation by forcing independence between different dimensions of  $\mathbf{z}$ , while reconstructing the input  $X$ . Inter-factor independence is achieved by minimising the Total Correlation (TC) objective imposed on the inferred latent vector [40].

A widely-used VAE that encourages disentanglement is the  $\beta$ -VAE [27]. Its main objective is the maximisation of the Evidence Lower-Bound Optimisation (ELBO), defined as:

$$\mathcal{L}(\theta, \phi; X, \mathbf{z}, \beta) = \mathbb{E}_{q_{\phi}(\mathbf{z}|X)}[\log p_{\theta}(X | \mathbf{z})] - \beta D_{KL}(q_{\phi}(\mathbf{z} | X) || p_{\mathbf{z}}), \quad (3)$$

where the first term corresponds to the input reconstruction error, and  $\beta > 1$  is used to regularise the Kullback-Liebler divergence ( $D_{KL}$ ) of the approximate posterior  $q_{\mathbf{z}|X}$  from the latent prior  $p_{\mathbf{z}}$ . Note that  $p_{\mathbf{z}}$  is usually a normal distribution with identity covariance matrix  $\mathcal{N}(0, \mathbf{I})$ . As argued by Rolínek *et al.* [41], the diagonal covariance forces a factorisation of the latent space where the factors are orthogonal, similarly to a PCA, which reasonably explains the disentanglement capabilities of VAEs [41, 42]. Intuitively,  $\beta > 1$  encourages disentanglement by forcing  $q(\mathbf{z} | X)$  to carry

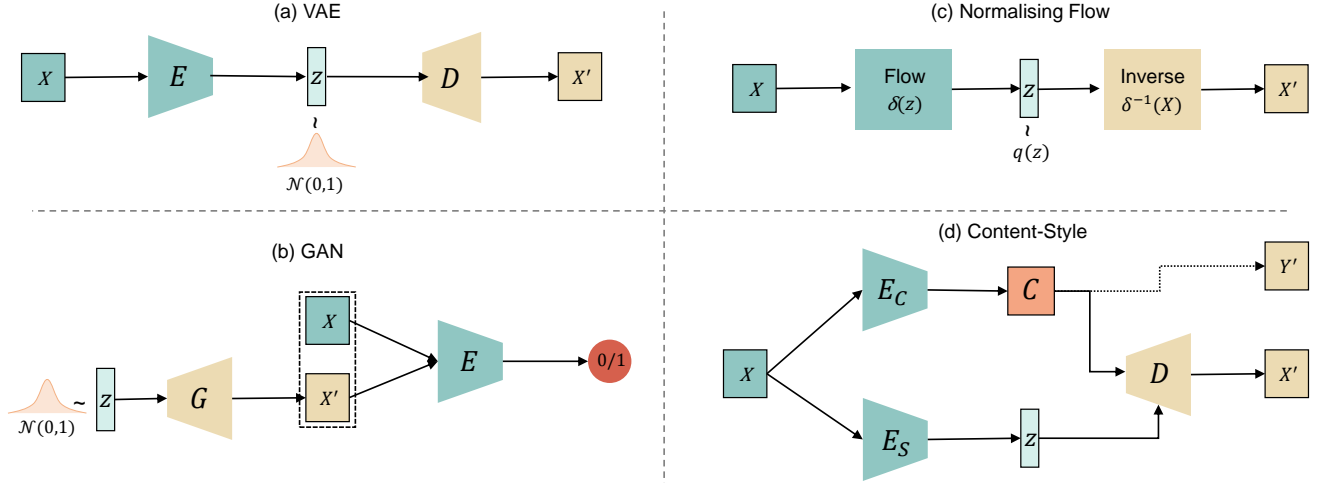


Fig. 2. Fundamental architectures for disentanglement: a) VAE, b) GAN, c) Normalising Flows, d) Content-Style disentanglement.  $X$  and  $X'$  are the input and reconstructed images.  $z$ ,  $C$  are the latent representations, where  $C$  represents a tensor latent variable (e.g. image content) and  $z$  represents a vector latent variable. The dashed line in (d) denotes the use of  $C$  for learning a representation  $Y'$  for a parallel equivariant task (e.g. semantic segmentation). Finally,  $\mathcal{N}$  denotes the normal distribution with zero mean and unit variance, whilst  $q(z)$  can be any prior distribution.

less information about the reconstruction by increasing the weight of the KL divergence term [42] and consequently, increasing independence between the factors of  $z$ .

Eq. 3 can be further augmented with the TC term that quantifies the redundancy and dependency between different dimensions of the latent vector. This term has been exploited by several VAE-based models [28, 29, 43].

### 3.2 Generative Adversarial Networks

An alternative to disentangling through reconstructing the input is image synthesis using Generative Adversarial Networks (GANs) [44]. As shown in Fig. 2(b), a GAN typically consists of a generator  $G$  and a discriminator  $D$  that play an adversarial game.  $G$  generates an image by sampling from an isotropic Gaussian distribution, while  $D$  is given the synthetic image and a real one ( $X$ ), and tries to identify which input is real/fake. The game is formalized as:

$$\min_G \max_D \mathcal{L}_{GAN}(G, D) = \mathbb{E}_{p(z)}[\log(1 - D(G(z)))] + \mathbb{E}_{p(X)}[\log(D(X))], \quad (4)$$

where  $z$  is a vector with values sampled from the aforementioned Gaussian and  $G(z)$  is the generated image.

In contrast to VAEs, the recent advances in GAN design and training settings have led to high-fidelity image generation [45, 46, 47]. GANs can learn disentangled representations by adding regularisation terms [23], by creating an architectural prior [45], or even by a post-hoc decomposition of the learned manifold after the training phase [48].

Regarding adding regularisation terms, a milestone approach is InfoGAN [23]. InfoGAN encourages disentanglement using two latent variables: a)  $z$  to encode the unstructured noise and b)  $c$  to learn the structured features of the data distribution. The disentanglement achieved by minimizing Eq. 4 objective, and by maximising the mutual information (MI) lower bound between  $c$  and the generated data. Cluster-GAN [49] extends the InfoGAN setting (adopting only the discrete version of c) by employing an inverse-mapping network to project the generated data back to the

latent space. This process is supervised by a clustering loss that operates as a regulariser.

Regarding architectural priors, the GAN structure introduced by Karras *et al.* [45, 50] includes a mapping network, which transforms the latent variable  $z$  into intermediate variables that control the style at each convolutional layer of the generator ( $G$ ). Interestingly, this enables feature manipulation at different levels of granularity, e.g. from shape down to texture. This hierarchical structure constitutes arguably a strong prior for disentanglement [51, 52].

### 3.3 Normalising Flows

Differently from the non-invertible VAEs and GANs, the Normalising Flows (NFs) are a family of invertible probabilistic models that can compute the exact –and not the approximated as in VAEs– likelihood [53, 54, 55, 56]. The NF framework derives from the change of variables formula in probability distributions [53]. Considering a variable  $X = \delta^{-1}(z)$ , where  $z \sim q(z)$  is sampled from a *prior* distribution  $q(z)$ , the posterior of  $X$  can be obtained by:

$$p(X) = p(z) \left| \det \frac{\partial \delta^{-1}}{\partial z} \right|^{-1}. \quad (5)$$

Note that the flow  $\delta : \mathbb{R}^d \rightarrow \mathbb{R}^d$  is constrained to be a *diffeomorphism*. Diffeomorphisms are differentiable and invertible transformations, with a differentiable inverse ( $\delta^{-1}$ ). When multiple flows ( $\delta_i^{-1}$ ) are combined in a chain, they can approximate arbitrarily complex densities for  $p(X)$ . As depicted in Fig. 2(c), one can use  $\delta$  to encode an image  $X$  into a latent space  $z$  or create a generative model by decoding a sample  $z \sim q(z)$  into image space using the inverse flow  $\delta^{-1}$ . The determinant of the Jacobian in Eq. 5 can be interpreted as a volume correction term. Therefore, the process of going from  $p(X)$  (e.g. image distribution) to  $p(z)$  (e.g. Gaussian distribution), gives the name of the NFs. Note that NFs have been recently adapted to encode disentangled representations [57, 58]. In fact, disentanglement is achieved by reinforcing similarity between latent spaces  $z$

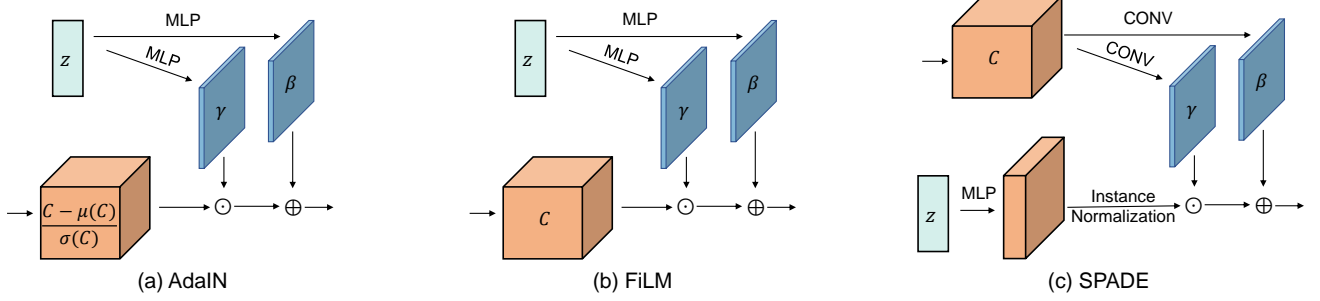


Fig. 3. Disentanglement building blocks that combine content  $C$  with style  $z$ : a) AdaIN, b) FiLM, and c) SPADE.  $\odot$  and  $\oplus$  denote element-wise multiplication and addition, respectively. MLP and CONV denote multilayer perceptron and convolutional layers.

of pairs of images with similar generating factors. We refer the reader to Kobyzev *et al.* [59] for a comprehensive review.

The aforementioned models typically decompose factors into a single vector representation. However, a more recent trend in disentanglement focuses on the decomposition of the input image into different latent variables that encode different properties, such as geometric vs. stylisation properties. Typically this approach entails the disentanglement of the image style and content, where content can be a spatial factor, while the style is still encoded as a vector. We discuss this type of disentanglement in the next section.

### 3.4 Content-Style Disentanglement

Another form of disentanglement is the so-called Content-Style Disentanglement (CSD) [60], where an image is decomposed into domain-invariant “content” and domain-specific “style” representations [61, 62]. Most works in CSD encode content in spatial (tensor) representations to preserve the spatial correlations and exploit them for a spatially equivariant task, such as Image-to-Image (I2I) translation [63, 64] and semantic segmentation [65]. The corresponding style, *i.e.* the information that controls the image appearance like colour and intensity, is encoded in a vector. An abstract visualisation of such a CSD model is depicted in Fig. 2(d). Note that decomposing content from style is not a trivial process, and encoding content as a high-dimensional representation is not enough. Recent work introduces several design (in terms of the model architecture) and learning (in terms of loss functions) biases to achieve this separation. We denote these inductive biases as “building blocks” and discuss them in the following section.

## 4 DISENTANGLEMENT BUILDING BLOCKS

Having detailed the fundamental concepts and models for disentanglement, we now proceed to report on common layers and modules that are used at various levels of the model design to encourage disentanglement. We associate these so-called building blocks with different high-level parts of the aforementioned AEs and generative models.

### 4.1 Encoder

The following layers are commonly used at various levels of the content encoder(s) in popular CSD architectures.

**Instance Normalisation.** Instance Normalisation (IN), originally proposed in [66] for style removal, is widely used

after each convolutional layer of the content encoder to suppress information related to style. In fact, IN removes any contrast-related information from each instance (data sample), encouraging the content-related features to be propagated to the following layers. An indicative example is the content encoder of [67], in which IN replaces all batch normalisation layers [68].

**Average Pooling.** Contrary to IN, average –or global– pooling is commonly used to suppress the content information in the style encoder [67]. In fact, by averaging the values and flattening a spatial feature to a vector, this operator removes any spatial correlation and encodes the global mean statistics (*i.e.* image style).

**Gumbel Softmax.** For CSD models that require semantic and parsimonious content to use it for a parallel spatially equivariant task, there is the need for discretisation of the encoded continuous information. The Gumbel Softmax operator is a differentiable solution to this problem. This operator mimics the reparametrisation trick performed in the VAE latent space (see Section 3.1) by sampling from a standard Gumbel distribution and using the Softmax as an approximation of the “argmax” step that is usually coupled with the one-hot operators for discretisation.

**Frequency Decomposition.** Recent studies have investigated the use of frequency decomposition transformations to encourage CSD. For example, Liu *et al.* [69] use the fast Fourier transform to extract image amplitude and phase. Intuitively, the former reflects image style, whereas the latter corresponds to image content. Huang *et al.* [70] use Discrete Cosine Transformation (DCT) to extract the domain invariant and domain specific frequency components, as an approximation of content and style factors, respectively.

### 4.2 Decoder

Apart from encouraging disentanglement during the encoding phase, effectively recombining the content and style representations in the decoder is also critical. The following layers are commonly used for this purpose at various levels of the decoder in popular CSD architectures.

**Adaptive Instance Normalisation.** The Adaptive Instance Normalisation (AdaIN) layer [67] is commonly used at multiple decoder levels to recombine the content and style representations. As depicted in Fig. 3(a), each AdaIN layer performs the following operation:

$$\text{AdaIN} = \gamma \frac{C_j - \mu(C_j)}{\sigma(C_j)} + \beta_j, \quad (6)$$



where each feature map  $C_j$  is first normalised separately, and then is scaled and shifted based on  $\gamma$  and  $\beta$ , which are parameters of an affine transformation of the style representation (adaptive mean and standard deviation).

**Feature-wise Linear Modulation.** As shown in Fig. 3(b), Feature-wise Linear Modulation (FiLM) [71] is similar to AdaIN. FiLM was initially proposed as a conditioning method for visual reasoning (the task of answering image-related questions). Using FiLM, each channel of the network’s intermediate features  $C_j$  is modulated based on  $\gamma_j$  and  $\beta_j$  as follows:  $FiLM(C_j|\gamma_j, \beta_j) = \gamma_j \cdot C_j + \beta_j$ , where element-wise multiplication ( $\cdot$ ) and addition are both broadcast over the spatial dimensions. It is used in [65] to combine the content and style in the decoder, where  $\gamma$  and  $\beta$  parameterise the affine transformation of style vectors.

**Spatially-Adaptive Denormalisation.** An alternative approach for combining content with style is the use of multiple Spatially-Adaptive Denormalisation (SPADE) [72] layers. As depicted in Fig. 3(c), a SPADE block receives the content channels and projects them onto an embedding space using two convolutional layers to produce the modulation parameters (tensors)  $\gamma$  and  $\beta$ . These parameters are then used to scale ( $\gamma$ ) and shift ( $\beta$ ) the normalised activations of the style representation.

### 4.3 Latent space

The following operations and priors can be applied on a latent space to encourage disentanglement.

**Gradient reversal layer.** The Gradient Reversal Layer (GRL) has been introduced in [73] in the context of domain adaptation, where the gradient is reversed to prevent the model from predicting undesired results. It has been shown that a GRL is effective in learning domain-specific style representations [74]. Specifically, when using the style from one domain to generate images with style from another domains, the gradient is reversed to prevent this happening.

**Concatenation.** Concatenating the content and style to form the input for the decoder is an alternative way of combining the two vector representations [64, 75]. Simple concatenation allows the content and style to be more flexible in capturing the desired information. However, this may limit the controllability of learning the content and style.

**Gaussian prior.** Encouraging the distribution of the encoded (vector) latent representation to match a Gaussian is a common prior. As reported in Sec. 3.1, such prior encourages the unsupervised disentanglement of the factors of variation and enables sampling for generating new images.

**Task priors.** As discussed in Sec. 3.4, content representation can be used for a downstream equivariant task, *e.g.* semantic segmentation. Task losses, such as the segmentation loss, also contribute at learning a disentangled content representation [65]. Other task-based priors, *e.g.* the number of human body parts [76], can be leveraged to encourage certain properties for the content.

### 4.4 Learning setups

Apart from the layers, operators, and priors, there are popular learning setups that can be leveraged to encourage disentanglement.

**Cycle-consistency.** Cycle-consistency [77, 78, 79, 80] is a technique for regularising image translation settings. In particular, cycle-consistency can be useful for reinforcing correspondence between input and generated images [81, 82], or to improve stability and reconstruction faithfulness in unsupervised and semi-supervised settings [83].

**Latent regression.** To ensure that the decoder does not ignore any latent variable (*e.g.* ignore style in a CSD setting), latent regression is employed to enforce the reconstructed image to contain information encoded into this representation [63]. In particular, considering an input image  $X$ , the disentangled style representation  $\mathbf{z}$  and the reconstructed image  $X'$ , we wish to extract a new latent representation  $\mathbf{z}'$  from encoding  $X'$ , which will be as similar as possible to  $\mathbf{z}$ . In other words, we need to minimise the distance between  $\mathbf{z}$  and  $\mathbf{z}'$  using a latent regression loss.

## 5 METRICS FOR DISENTANGLEMENT

To understand disentanglement and design models that improve it, we need to be able to quantify how disentangled is (are) the encoded representation(s). Below, we briefly report the most popular disentanglement metrics splitting them into 2 categories: i) disentanglement of factors in a single vector latent variables, and ii) disentanglement between two latent variables of the same or different dimensionality.

**Single vector-based latent variable.** This category consists of both qualitative and quantitative methods for measuring disentanglement.

Qualitatively, we can evaluate disentanglement by traversing a single latent dimension that alters the reconstructed image by a single aspect (*e.g.* increase image intensity). These traversals are practically linear interpolations that allow us to perform “walks” in non-linear data manifolds and to interpret the variation controlled by each factor [84, 85]. Latent traversals do not require ground truth information about the factors.

Quantitatively, there has been considerable effort to quantitatively evaluate vector representations. As there are different proxies for disentanglement, popular metrics focus on different aspects of measuring it. For example, Higgins *et al.* [27] propose the first metric to quantify disentanglement when the ground truth factors of a data set are available. In fact, they evaluate disentanglement using the prediction accuracy of a linear classifier that is trained as follows; they first choose a factor  $k$  and generate data with this factor fixed, but all others varying randomly. After obtaining the representations of the generated data, they take the absolute value of the pairwise differences of these representations. Then the mean of these statistics across the pairs gives one training input for the classifier, and the fixed factor index  $k$  is the corresponding training output. Subsequently, Kim *et al.* [29] adopt the metric of [27], but construct the training set of the linear classifier by considering the empirical variance of normalised representations rather than the pairwise differences. Chen *et al.* [28] argue that given a factor of variation, the first two dimensions of the latent vector should have the highest MI. They measure the gap between these two dimensions using the introduced mutual information gap metric. Ridgeway *et al.* [25] propose to measure the modularity of latent representations by measuring

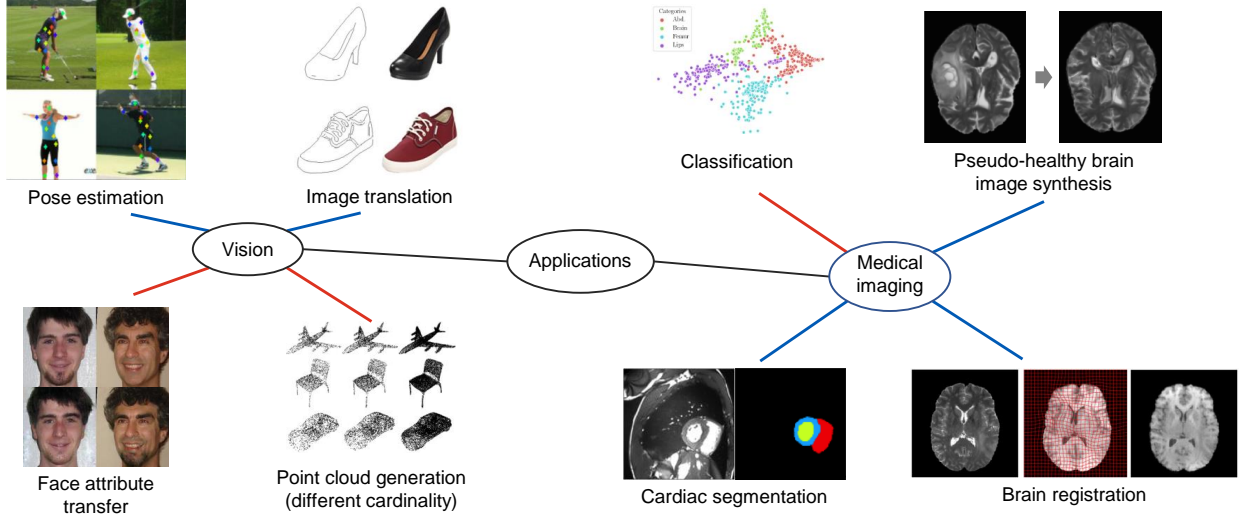


Fig. 4. Visual summary of disentangled representation learning applications in the computer vision (left) and medical imaging (right) domains. Red connections indicate vector-based disentanglement, while blue connections indicate tensor/vector-based one (CSD). The visual examples are taken from the respective works cited and detailed in Section 6.

the MI between factors, ensuring that each vector dimension encodes at most one factor of variation. Eastwood and Williams [24] first train an encoder on a synthetic dataset with predefined factors of variation  $z$ , and encode a representation  $c$  for each data sample. Then, they train a regressor to predict each factor  $z$  given a  $c$  representation. Based on the prediction accuracy, they measure the disentanglement, completeness, and informativeness of each representation. Finally, Kumar *et al.* [86] propose the separated attribute predictability score to first compute the prediction errors of the two most predictive latent dimensions for each factor, and then use the average error difference as a disentanglement metric. A more comprehensive review of metrics for disentanglement in vector space can be found in [87].

**Two latent variables.** The aforementioned metrics are not applicable in CSD as they rely on either having ground truth for factors of variation or assuming that the latent manifold is solely vector-based. To evaluate CSD one should consider more than one latent variables and a possible difference in dimensionality, *e.g.* the case of spatial content (tensor) and vector style. To the best of our knowledge, the only work that focuses CSD metrics is the one of Liu *et al.* [88]. In this work, the authors consider the properties of uncorrelation and informativeness, and propose to combine the empirical distance correlation [89] and a metric termed information over bias, to measure the degree of disentanglement *between* content and style representations. Two other methods for measuring the uncorrelation-independence between variables of different dimensionality are the kernel-target alignment [90] and the Hilbert-Schmidt independence criterion [91]. However, both methods require pre-defined kernels.

## 6 APPLICATIONS OF DISENTANGLEMENT

In the previous section we provided a thorough analysis of the fundamental concepts and the building blocks of disentangled representation learning. *But is disentanglement relevant to real-life applications?* Here, we answer this question by

reporting details of exemplar methods that exploit disentanglement to improve challenging tasks in two major domains: computer vision and medical image analysis. Since it is impossible to discuss every task and every available method for each domain, we pick exemplars and detail the architecture, training setup, utilised data, and implementation tips and tricks. All URLs of official implementations for the highlighted methods can be found in the associated repository [https://github.com/vios-s/disentanglement\\_tutorial](https://github.com/vios-s/disentanglement_tutorial). A visual summary of this section is depicted in Fig. 4.

### 6.1 Computer vision

#### 6.1.1 Image-to-image translation

Translating an image representation into another, which differ in a specific characteristic (*e.g.* style) is termed I2I translation. Although there are several models that showcase impressive results in this task, the Multimodal Unsupervised Image-to-image Translation (MUNIT) [63] model is the first to incorporate CSD paradigm into and has become a widely adopted benchmark.

**Architecture.** The basic assumption is that multi-domain images share common content information, but differ in style. A content encoder maps images to multi-channel feature maps, by removing style with IN layers [66]. A second encoder extracts global style information with fully connected layers and average pooling. Finally, style and content representations are combined in the decoder through AdaIN modules [67]. Disentanglement is further encouraged by a bidirectional reconstruction loss [92] that enables style transfer. In order to learn a smooth representation manifold, two latent regression losses are applied on content and style extracted from input images, namely a content-based latent regression loss that penalises the distance to the content extracted from reconstructed images, and a style-based latent regression that encourages the encoded style distributions to match their Gaussian prior. Finally, adversarial learning encourages realistic synthetic images.



**Training setup.** MUNIT achieves unsupervised multi-modal image-to-image translation by minimising the following loss function:

$$\mathcal{L}_{total} = \mathcal{L}_{GAN} + \lambda_1 \mathcal{L}_{rec} + \lambda_2 \mathcal{L}_{c-rec} + \lambda_3 \mathcal{L}_{s-rec}, \quad (7)$$

where  $\mathcal{L}_{rec}$  is the image reconstruction loss,  $\mathcal{L}_{c-rec}$  and  $\mathcal{L}_{s-rec}$  denote the content and style reconstruction losses, and  $\lambda_1 = 10$ ,  $\lambda_2 = 1$  are the hyperparameters used by the authors. The model has been evaluated on SYNTHIA [93], Cityscapes [94], edge-to-shoes [95], and summer-to-winter [96] datasets.

**Tips & Tricks.** MUNIT has shown robust and impressive performance on multiple I2I scenarios. The style representation is sampled directly from  $N(0, 1)$ , which means the style latent space is smoother and better for style traversal compared to the style learned by minimizing KL divergence using the re-parameterization trick (introduced in [36]). Assuming a semantic content prior, the AdaIN layers in the decoder can be replaced with the SPADE module to achieve more controllable translation. The provided hyperparameters can be used for most datasets, without needing intensive tuning. The major drawback of MUNIT is the vague definition of content *i.e.* domain-invariant representation, which is achieved by the bi-directional reconstruction. The content is not interpretable and it is not trivial to measure how domain-invariant the content is.

**Other works.** Other popular models that adopt disentanglement for I2I are: a) DRIT [97] and cd-GAN [98] with a setting similar to MUNIT, b) TransGaGa [99] that models content as landmark heatmaps, and c) the model proposed in [100] for contrastive unpaired translation by enforcing patch-wise content consistency.

### 6.1.2 Face attribute transfer

The task of facial attribute transfer is defined as the generation of a synthetic face that contains the targeted attribute, but without altering the subject identity (*e.g.* adding bangs to a subjects forehead). Most methods that focus on facial attribute transfer struggle with; a) transferring more than one attributes at a time, b) generating images based on exemplars, and c) achieving high-fidelity results. As an exemplar we use ELEGANT [101], the first model to address the aforementioned challenges by encoding disentangled attribute representations of two exemplars in a vector latent space and performing attribute swapping.

**Architecture.** ELEGANT consists of a U-Net [102] like architecture with vector-based latent space and receives two face image samples; one positive sample  $X_A$ , *i.e.* a face that contains the desired attribute, and a negative one  $X_B$  that can contain any other attribute except for the targeted one. The exemplar face attributes are encoded into disentangled vector representations  $\mathbf{z}_A$  and  $\mathbf{z}_B$  of the same predefined dimensionality, where to generate exemplar variants the authors swap the  $i^{th}$  value (which encodes the desired face attribute) between  $\mathbf{z}_A$  and  $\mathbf{z}_B$ , creating  $\mathbf{z}_C$  and  $\mathbf{z}_D$  representations. These representations are combined to generate (or reconstruct) four images; a) exemplar  $X_A$  is reconstructed from the concatenation of  $\mathbf{z}_A$  with itself, b)  $X_{A'}$  is a variant of  $X_A$  that includes the desired attribute from exemplar  $X_B$ , which is generated from concatenating  $\mathbf{z}_A$  and  $\mathbf{z}_C$ , c)  $X_B$  is reconstructed from  $\mathbf{z}_B$  concatenation with itself, and d)

$X_{B'}$  is a variant of  $X_B$  that includes the desired attribute from exemplar  $X_A$ , which is generated from concatenating  $\mathbf{z}_B$  and  $\mathbf{z}_D$ . It should be noted that the model’s residual connections are used to provide the additional context for each generated image, as the mixed  $\mathbf{z}$  representations provide information for the local area that is correlated with the swapped attribute. Apart from the autoencoder, the method uses two discriminators  $D_1$  and  $D_2$  that operate into different image scales to learn to generate both realistic overall content and fine-grained detail.

**Training setup.** Identifying the U-Net part as a generator, ELEGANT is trained as a typical GAN model, minimising the following loss function for the two discriminators:

$$\mathcal{L}_D = \mathcal{L}_{D_1} + \mathcal{L}_{D_2}, \quad (8)$$

where  $\mathcal{L}_{D_1}$ ,  $\mathcal{L}_{D_2}$  correspond to the typical adversarial loss for the discriminators, while the following loss function is used to train the generator:

$$\mathcal{L}_G = \mathcal{L}_{rec} + \mathcal{L}_{adv}, \quad (9)$$

where  $\mathcal{L}_{rec}$  is the  $\ell_1$  loss computed for  $X_A$ ,  $X_{A'}$  and  $X_B$ ,  $X_{B'}$ , and  $\mathcal{L}_{adv}$  corresponds to the typical adversarial loss for the generator. The model has been evaluated on CelebA which consists of 40 facial attributes and 5 landmarks annotations. The authors use these landmarks to align all faces and center-crop a  $256 \times 256$  region.

**Tips & Tricks.** The authors use the same encoder and decoder to produce the vector representations for the two input faces and generate the four possible combinations. However, each subject has its own discriminator. To avoid batch normalization, which would smooth the differences between two facial images,  $\ell_2$ -normalization is used across the U-Net and both discriminators. ELEGANT is smooth to train due to the residual connections that lower the burden of the generation process as the decoder focuses only on the synthesis of the swapped-in characteristic. Finally, as noted by the authors, for resolutions of  $256 \times 256$  and higher, multi-scale discriminators can significantly contribute to the synthetic image quality.

**Other works.** Lin *et al.* [103] propose a GAN model with a domain classifier to learn to transfer attributes between multiple domain. He *et al.* [104] present a GAN architecture that conditions the face generation of opposite samples (*e.g.* smile, no smile) using one-hot attribute vectors. Zhou *et al.* [105] exploit cycle consistency to transfer attributes, with the limitation that the attributes should be located approximately at the same spatial location.

### 6.1.3 Pose estimation

The human body constitutes a strong content prior that can be exploited to encode body structure in a spatial and semantic latent space, to be used for equivariant tasks that require body joint position. Lorenz *et al.* [76] propose a model that uses this type of disentanglement for the challenging articulated body pose estimation task.

**Architecture.** The proposed model is a dual-stream autoencoder that disentangles the body pose from the image appearance. The body pose is represented as a multi-channel feature map, where each channel corresponds to a specific body part. A Gaussian distribution is applied to

each feature map to remove any style information, while also preserving the spatial correspondence. The corresponding appearance information is extracted from the encoder features using average pooling. Note that the style vectors do not correspond to global image style, since they are applied to specific content parts during decoding. Disentanglement is further encouraged with a transformation equivariance loss, which ensures that the spatial transformations, *i.e.* translations and rotations, affect only the content representation, while the intensity ones, such as the colour and texture information, affect only the corresponding style.

**Training setup.** The dual-stream model is trained in an unsupervised way by minimising the loss:

$$\mathcal{L}_{total} = \lambda_1 \mathcal{L}_{rec} + \lambda_2 \mathcal{L}_{equiv}, \quad (10)$$

where  $\mathcal{L}_{rec}$  is the mean absolute error between the reconstructed and the input image.  $\mathcal{L}_{equiv}$  is the equivariance loss, which ensures that the mean and covariance of the parts coordinates do not change after some style transformation. During training the authors set  $\lambda_1 = \lambda_2 = 1$ . The model has been evaluated on Human3.6M [106] and Penn Action [107] human activity datasets. For the former, the background subtraction method provided in the dataset is used to keep the (foreground) human body information, while for the latter the authors crop the samples around the human body using the provided bounding boxes, and then resized the results to  $128 \times 128$  pixel resolution.

**Tips & Tricks.** The content learned by this model is highly interpretable [88]. When training this model, visual observation on the content representation provides a way to measure if the model is well trained when no annotations are given. The content and style in this model are well disentangled as analysed in [88], which means this model is powerful on generating plausible images by modulating the content and style. The model is heavily biased to the task *e.g.* the number of content channels is the number of body parts and the content is modeled by the Gaussian blobs. Moreover, the content and style are learned by enforcing equivariance to designed spatial and intensity transformations, which is limited by the adopted transformations.

**Other works.** Esser *et al.* adopt the disentanglement of the human body pose from the corresponding appearance (style) information in the context of a dual-encoder VAE setting, however they use the body-related factors for other human appearance transfer [75] and synthesis [108].

#### 6.1.4 Point cloud generation

Several methods for generating set-structured data, such as point clouds, adopt multi-scale and sequential learning frameworks. However, since set-structured samples must be invariant to the permutation of their elements, it is not trivial to directly exploit these frameworks. A critical element-oriented permutation in point clouds is the change of cardinality. To address the variability of cardinality in point cloud generation, Kim *et al.* [109] propose a hierarchical VAE that disentangles the cardinality of the input set from the rest of the generative factors (SetVAE). We choose this model as it is the only one that disentangles cardinality as a factor and achieves state-of-the-art performance in several metrics.

**Architecture.** SetVAE structure, which is inspired by well-known hierarchical VAEs [110, 111], is composed by

a bottom-up encoder and a top-down decoder sharing the same dependency structure. The encoder consists of multiple stacked Induced Set Attention Blocks (ISAB, introduced in [112]), each of them producing a permutation-invariant deterministic encoding  $h$  of the input set. On the other hand, the decoder consists of stacked attentive bottleneck layers that extend the structure of ISAB by stochastically interacting with the latent variable  $z$ . Note that  $z$  is not sampled by a Gaussian prior, but from a distribution conditioned by the corresponding  $h$  (*i.e.* from the same hierarchical layer).

**Training setup.** The authors train SetVAE by minimising:

$$\mathcal{L}_{SetVAE} = \mathcal{L}_{rec} + \beta \mathcal{L}_{KL}, \quad (11)$$

where  $\mathcal{L}_{recon}$  denotes the proxy reconstruction loss (Chamfer Distance) computed between the generated point-cloud and the input, and  $\mathcal{L}_{KL}$  is the Kullback-Leibler divergence between the multi-layer (based on the formed hierarchy) approximate posteriors and their corresponding priors. The hyperparameter  $\beta$  is used to normalise the KL values with respect to the Chamfer Distance. The model is evaluated using 3 datasets of different complexity; a) ShapeNet [113], b) Set-MNIST [114], and c) Set-MultiMNIST [115] datasets.

**Tips & Tricks.** SetVAE is a cascade of transformer models, where the distribution of the latent vector space is encouraged to match a (factorised) Gaussian one. For smoother and faster convergence during training, instead of a unimodal Gaussian prior for the 0-cardinality element distribution, the authors propose the use of mixture of Gaussians. Another tip for smoother training is the parameter sharing between the attentive layers of the inference and generation modules (see Fig. 3 in [109]). Finally, to prevent the loss of attention in some parts of the input point-cloud, the authors enhance the attention score calculation with the slot attention method [116], which ensures that no attention value is zero, thus not input element is ignored.

**Other works.** Point cloud, and in general set-based, generation has been approached by several methods, however only PointFlow [117], which is based on NFs, disentangles the cardinality of the input.

## 6.2 Medical image analysis

Medical applications can specially benefit from disentangled architectures due to lack of available data and ability for semi-supervised learning. This potentially increases training dataset bias in situations such 1) data are acquired by similar machines but need to be tested in a wild variety (acquisition shift); 2) one pathology is more frequent than another (population shift); 3) data come from few institutions [20]. This makes approaches more susceptible to failures at test time due to domain shifts. In this setting, explicitly defining models that are in(equi)variant to specific changes in the input data can be useful.

### 6.2.1 Single-modal Segmentation

Regarding single-modal medical image segmentation, the input images have one modality *e.g.* MRI images. The target is to train a model to accurately predict the pixel-wise labels (segmentation mask) with the image as input. For this task, the most widely used model is Spatial Decomposition Network (SDNet)[65], which decomposes 2D medical images

into spatial anatomical factors (content) and non-spatial modality factors (style).

**Architecture.** SDNet uses two different encoders for factorising content into a spatial representation and style into a vector one. A decoder is responsible for reconstructing the input by combining the two latent variables, while a segmentation module is applied on the content latent space to learn to predict the segmentation mask for each cardiac part. SDNet learns the content which is represented as multi-channel binary maps of the same resolution as the input. This is obtained with a softmax and a thresholding function [118]. To encourage the style encoder to encode only style-related information, the authors employ a VAE network. Then, style and content are combined to reconstruct the input image by applying a series of convolutional layers with FiLM layers [71].

**Training setup.** SDNet is trained by minimising the following loss function:

$$\mathcal{L}_{total} = \lambda_1 \mathcal{L}_{KL} + \lambda_2 \mathcal{L}_{seg} + \lambda_3 \mathcal{L}_{rec} + \lambda_4 \mathcal{L}_{z_{rec}}, \quad (12)$$

where  $\mathcal{L}_{KL}$  is the KL Divergence measured between the sampled and the predicted style vectors,  $\mathcal{L}_{rec}$  is the image reconstruction loss,  $\mathcal{L}_{seg}$  is the segmentation loss, and  $\mathcal{L}_{z_{rec}}$  is the latent regression loss between the sampled and the re-encoded style vector.  $\lambda_1 = 0.01$ ,  $\lambda_2 = 10$ ,  $\lambda_3 = 1$ , and  $\lambda_4 = 1$  are the hyperparameters used by the authors. SDNet has been evaluated on the ACDC [119], MM-WHS [120, 121, 122], and M&Ms [123] cardiac datasets, as well as on the SCGM [124] spinal one.

**Tips & Tricks.** SDNet encodes highly semantic content representation, which shows the advantage of content interpretability. Additionally, the variational encoding of the style representation allows for sampling and interpolation of the appearance factors, enabling the synthesis of new plausible images [125]. Other modifications include using a SPADE module to replace FiLM, which has led to a performance improvement in several studies [88, 126]. Gumbel-Softmax [127] can replace the naive softmax [126] and binary thresholding. When temporal information is available, temporal consistency objectives can be applied to boost the performance as in [128]. To learn generalisable representations, gradient-based meta-learning can be applied as a leaning strategy when giving multi-domain data [129].

**Other works.** Recent disentanglement methods focus in segmentation in the context of federated learning [69, 130] and joint image-label distribution modeling [131].

### 6.2.2 Multi-modal and cross-modal segmentation

For multi-modal or cross-modal medical image segmentation, at least two modalities are required (e.g. CT and MRI scans). Our goal is accurately predict the pixel-wise class labels (segmentation mask) given a specific patient, exploiting both (all) available modalities. For this task, MUNIT [63] is the most popular model.

**Architecture.** Typically, there are two ways of using MUNIT for multi-modal or cross-modal medical image segmentation. The first strategy is aligning the content spaces of data from different modalities e.g. CT and MRI [132, 133, 134, 135, 136]. Then, a segmentation network is used to predict the mask with content representations as input. Alternatively, the scenarios of imbalanced domains

and domain adaptation is considered, where there is a domain with more data and annotations (e.g. MRI) and a domain with less data and few or no annotations (e.g. CT) [137, 138]. After training a MUNIT model on the two domains, the translation mappings between them can be obtained. During inference, the samples from CT domain are initially translated to MRI scans, which are then used to predict the segmentation mask by a segmentor trained on the MRI domain. MUNIT has been evaluated on the following medical datasets: LiTS [139] liver, NCANDA [140] and BraTS [141] brain, CHAOs [142] abdomen organs, and MS-CMRSeg [143, 144] and MM-WHS [120, 121, 122] cardiac datasets, respectively.

**Tips & Tricks.** First, the consistency losses can be applied on the task output. For example, the predicted segmentation masks of the original MRI scan and the corresponding translated CT-style images must be consistent [145]. Further, the anatomical (content) latent variables of the different modalities can be aligned or fused by applying adversarial training [138] and prior constraints as in [135, 136, 146]. Compared to SDNet, MUNIT’s disentangled content is less interpretable, while it needs to be trained using a bi-directional setup. This means that it cannot be used for single-modal datasets.

**Other works.** Other works on multi-modal segmentation include the use of CT data to improve segmentation performance on cone beam computed tomography scans [147], as well as the exploitation of aligned Cine and LGE data [146].

### 6.2.3 Image synthesis

Many medical imaging procedures are expensive to perform, are invasive and uncomfortable for patient. For this reason, datasets of certain modalities are usually small and imbalanced. To address these problems, medical image synthesis is considered for augmenting and balancing these datasets. Besides, some images are impossible to acquire: doctors might wish to have an image of patient when the patient was healthy in order to perform a comparative diagnosis [82, 148] (these hypothetical image estimations are also called counterfactuals).

A recent work that focuses on image synthesis by exploiting disentangled representation is the one of Xia *et al.* [82], which includes a comprehensive evaluation and comparison with related works. Xia *et al.* explore disentanglement in the context of synthesising pseudo-healthy brain MRI from patients with tumors or ischemic stroke lesions. The pathology information is disentangled from anatomical features as a segmentation mask. Note that many of the ideas presented in this paper can be easily translated to other organs and relevant tasks.

**Architecture.** In their framework, a generator ( $G$ ) extracts a healthy image from a pathological image, and a segmentor ( $S$ ) extracts the remaining pathological information as a mask. Subsequently, a decoder module  $R$ , which is responsible for reconstructing the input, receives and combines the extracted healthy image and mask enforcing consistency between input and reconstruction. Each sub-network consists of a U-net like architecture with residual blocks and sigmoid output activation, while there are also two discriminators for the healthy images and masks.

**Training setup.** Two discriminators enforce the (generated) healthy images and the masks to be realistic ( $\mathcal{L}_{GAN_1}$  and  $\mathcal{L}_{GAN_2}$ ). When ground truth masks are available, a DICE score is used to learn the segmentations ( $\mathcal{L}_{seg}$ ). Otherwise, adversarial training allows semi-supervised learning of the segmentation with unpaired masks. A cycle-consistency loss ( $\mathcal{L}_{CC_1}$ ) ensures that the subjects keep the “identity”. The goal is to solely change the pathological aspect while preserving patient identity. Therefore, an additional ( $\mathcal{L}_{CC_2}$ ) cycle consistency objective is introduced to prevent the generator from making unnecessary changes (e.g. generation of pathologies for healthy images). The final loss is a combination of the above losses:

$$\mathcal{L}_{total} = \lambda_1 \mathcal{L}_{GAN_1} + \lambda_2 \mathcal{L}_{GAN_2} + \lambda_3 \mathcal{L}_{CC_1} + \lambda_4 \mathcal{L}_{CC_2} + \lambda_5 \mathcal{L}_{seg} \quad (13)$$

The model is evaluated on the following datasets: ISLES [149], BraTS, and Cam-CAN [150] brain datasets.

**Tips & Tricks.** The main bias introduced in Xia *et al.* [82] is the use of an auxiliary network for guide synthesis in a cycle consistency setting. In addition, they observed that, in practice, using a Wasserstein loss coupled with gradient penalty [151] is more beneficial compared to the Least Squares discriminator loss [152].

**Other works.** Other applications include metal artifacts reduction [153], speckle noise reduction [154], multi-modal synthesis [155, 156, 157], disease decomposition [82, 148, 158, 159], explainability [160], controllable synthesis [126, 161, 162, 163, 164], and image harmonisation [165, 166].

#### 6.2.4 Causal Image Synthesis

Causal image synthesis [167, 168] is a special case of conditional generation where the conditioning architecture follows a SCM. The representation of each causal variable needs to be disentangled and their relation should be specified by the designer. This is a stronger form of bias than disentangling variables only.

Initial work in this direction has been done by Pawlowski *et al.* [167], constructing a causal model capable of performing counterfactuals with imaging data. A causal graph for a brain MRI problem is constructed where the brain ventricular volume depends on the age, but not on the patient’s sex.

**Architecture.** Pawlowski *et al.* rely on NFs [54] (invertible neural models (section 3.3) for modeling attributes such as age, sex, brain and ventricular volume and their relationships; and conditional VAEs for synthesising imaging counterfactuals. The conditionals follow a structure based on clinical knowledge about the problem. The authors enable counterfactual estimation by using invertible models. It allows the prediction of a latent representation of an observation and sequentially performing a local intervention by changing the desired latent space.

**Training setup.** The networks associated with the NFs and VAEs are trained jointly with backpropagation using the ELBO as a loss function. The model has been evaluated on brain MRI scans from the UK Biobank [169].

**Tips & Tricks.** The main method used for reinforcing the structural biases is NF, which are based on neural spine flows [170]. Additionally, the authors realised that normalisation as a pre-processing step is necessary, as it prevents the

learning of dependencies on the variable with the largest magnitude, while helping in combining the scalar attributes with imaging information. The implementation was done using the Pyro library [171] which can be useful for several probabilistic programming tasks.

**Other works.** CausalGAN [172] introduced generative models following a causal structure, however, they were not capable of estimating counterfactuals. Reinhold *et al.* [168] extend Pawlowski *et al.* [167] with linear rational splines and higher resolution images [173].

#### 6.2.5 Classification

A classification task and domain knowledge can be used to disentangle both task-specific representation  $\mathbf{z}_c$  from a classifier and task-agnostic representation  $\mathbf{z}_a$  [174, 175, 176]. By decoding both representations after a merging operation, one can reconstruct the image.

We use as exemplar the Mutual Information-based Disentangled Neural Networks (MIDNet) model proposed in [176], which was initially developed for ultrasound fetal imaging. Whilst building on earlier work [175], this approach leverages components that can be easily adapted to other applications and offers a multi-task framework to disentangled task-specific representations. Note that the main goal of disentanglement is to find representations that are invariant to different tasks and domains.

**Architecture.** The neural network is composed by two encoders  $E_c$  and  $E_a$ , a classifier  $C$  that takes  $\mathbf{z}_c$  as input and output the desired class, and a decoder to reconstruct the images by re-entangling the latent spaces  $\mathbf{z}_c$  and  $\mathbf{z}_a$ .

**Training setup.** Besides classification  $\mathcal{L}_{cls}$  and reconstruction  $\mathcal{L}_{rec}$  losses. They disentangle  $\mathbf{z}_c$  and  $\mathbf{z}_a$  using Mutual Information Neural Estimation (MINE) [177] ( $\mathcal{L}_{MI}$ ). Domain invariance in the  $\mathbf{z}_c$  latent is further reinforced via a clustering loss  $\mathcal{L}_{clus}$  that encourages samples from different domains, but with same label, to have similar task-specific representations. Finally, the network is trained in a semi supervised way ( $\mathcal{L}_{SSL}$ ) using the MixMatch method [178]. add an alignment loss for improving generalisation in a domain adaptation setting. The total loss is:

$$\mathcal{L}_{total} = \lambda_1 \mathcal{L}_{rec} + \lambda_2 \mathcal{L}_{cls} + \lambda_3 \mathcal{L}_{MI} + \lambda_4 \mathcal{L}_{clus} + \lambda_5 \mathcal{L}_{ssl}. \quad (14)$$

The method is evaluated using fetal ultrasound datasets.

**Tips & Tricks.** The main inductive bias in Meng *et al.* [176] is the definition of class specific and class agnostic representations. In addition, the authors use MINE [177], which is a learned loss function, for disentangling the two vectors. Other differentiable metrics such as the Hilbert-Schmidt Independence Criterion [91] could also be used as done in Liu *et al.* [129].

**Other works.** We refer the readers to other works [174, 179, 180, 181] where, for example, Berenguer *et al.* [180] train a conditional VAE to pre-train an encoder for the subsequent diagnosis classification task. Zhao *et al.* [181] learn a representation which projection is disentangled and Jung *et al.* [182] use capsules, both resulting in better representations for a downstream classification task.

#### 6.2.6 Registration

Image registration constitutes an important pre-processing step in medical image analysis. It is defined as the alignment

of the content of two images based on a transformation. This transformation can be parametrised by either an affine matrix (rigid) or by a displacement field (non-rigid). An important challenge is to define a cost function for multi-model cases; for example, comparing MRI and ultrasound scans using pixel-level metrics is not effective since the intensity, view and artifacts are different.

The work of Chen *et al.* [183] addresses this problem by leveraging CSD (section 3.4). In particular, they use a CNN to estimate the displacement field from the content space of two images (from different modalities). We choose to discuss this work as it is the first paper to leverage disentanglement for the task of medical image registration.

**Architecture.** Initially, a system based on the DRIT [64] architecture is used for image-to-image translation between two images of different domains. Then, they used the content  $E^c$  and style  $E^s$  encoders for each domain  $\mathcal{X}_i$ . Secondly, the content representations from two images are fed into a registration network  $G_{reg}$  that outputs deformation fields mapping one image to the other.

**Training setup.** A first training of the CSD is done as defined in Lee *et al.* [64]. Then, the registration network is learned by computing a bidirectional loss function based on the content latent space of the deformed images plus a regularisation loss over the latent space. The method is evaluated on lung CT scans from the COPDGene [184] dataset and brain MRI from the BraTS corpus.

**Tips & Tricks.** The main inductive bias used by this model is the fact that registration only depends on the image content, the style can be ignored. In addition, preservation of topological information is an important constraint in medical image registration. The authors use a Huber loss over the gradients of the deformation field for this purpose, reinforcing smoothness of the deformation field.

**Other works.** Chartsias *et al.* [146] use the disentangled anatomical factors to register the cine- with the LGE-MRI scans of the same patient.

## 7 OPPORTUNITIES AND OPEN CHALLENGES

In this section, we summarise opportunities for improving or further exploiting DRL, as well as various challenges to be addressed by the community.

**Self-supervised and contrastive learning.** Recently, contrastive learning [185, 186, 187, 188, 189] has shown impressive performance on self-supervised representation learning. In particular, [190, 191] have developed an understanding of contrastive learning from a causal perspective and have shown that it can be interpreted as CSD where the representation is focusing on learning only the content, whilst developing style invariance. Methods such as MOCO [185], SimCLR [186, 187], BYOL [188], and the Barlow Twins [189] achieve this mostly through augmentation and regularisation. While it is possible to learn representations that are robust (invariant) to specific interventions, it remains challenging to design augmentations and regularisations invariant to general interventions.

**Domain generalisation.** Domain generalisation considers that no information from the target domain is available and that a model trained on multiple source domains needs

to generalise well to the unseen target domain [192]. Although disentangled representations should be general, a recent study found that disentanglement does not imply guaranteed generalisation ability [193]. To address this, Meng *et al.* [176] use task-specific representations and feature clustering to achieve domain invariance, and Liu *et al.* [129] use meta-learning to explicitly improve domain invariance in disentangled representations. Learning robust and generalisable representations remains an open and under-explored problem.

**Measuring disentanglement.** As analysed in [21], most of the metrics reported in Sec. 5 require ground truth for each latent factor and do not perform consistently for different tasks and datasets. In addition, although CSD has attracted significant attention, with the exception of the ones proposed in [88], we currently lack metrics to measure disentanglement between multiple latent variables of the same or different dimensionality. The development of metrics that address these drawbacks is still an open challenge.

**Complexity.** Most architectures in the disentanglement literature use multiple loss functions and modules, as seen in section 6, which leads to multiple hyperparameters. While flexibility is desirable, tuning complex systems can be difficult and it creates a barrier for further adoption of the disentanglement paradigm by the broader research community. Therefore, developing methods that require less tuning or techniques for automating this process is still an open challenge.

**Interventions.** Caselles *et al.* [18] suggest that symmetry-based understanding of disentanglement can only be achieved upon interaction with an environment. Illustrating this point, Suter *et al.* [194] propose a disentanglement metric based on interventional robustness. Moreover, statistical independence between latent variables might not hold for real-life settings where the generating factors have causal relations. With this intuition, Besserve *et al.* [19] provide a causal understanding of disentanglement in generative models based on interventions and counterfactuals. We believe that these works have paved the path for using interventions as a prior for DRL.

**Compositionality.** As reported in Sec. 3.4, in the current CSD framework the content is vaguely defined as domain-invariant [67], task-equivariant [76] or even simply as spatial and binary [65]. These definitions usually point to the task-driven model designs for learning the desired content, which are limited to specific datasets or tasks. However, enforcing compositionality can be the solution for learning generalisable and robust content representations. This intuition is based on the compositional nature of the human recognition system, which is robust for recognising new concepts by composing the individual components [195]. We believe that the incorporation of compositionality into disentanglement is a great opportunity.

**Privacy-preserving disentanglement.** DRL has just started to be leveraged for maintaining privacy by becoming invariant to private features [130, 196, 197]. Considering that the privacy issues in machine learning have attracted significant attention [198], we believe that there is a new, emerging domain for learning privacy-preserved disentangled representations. As for every new domain, it will be challenging to connect and exploit the existing concepts,



such as the differential privacy [199] and the federated learning [200], with the disentanglement paradigm.

## 8 CONCLUSION

Overall, disentangled representation learning is a tool for introducing inductive biases (expert knowledge) into deep learning settings in order to simulate real-life scenarios with non-i.i.d. data. In this tutorial, we have reviewed methods for implicitly or explicitly forcing representations to be invariant or equivariant to specific changes in the input data. The goal is not to survey all existing work, but to give the reader the building blocks for introducing disentanglement in a diverse set of tasks. In summary, disentanglement can be achieved by one or both of modifications in the model architecture (e.g. MUNIT, StyleGAN) and regularisation constraints (e.g.  $\beta$ -VAE). We highlight that disentanglement can be especially useful in low data regimes where biases are more relevant.

## ACKNOWLEDGMENTS

This work was supported by the Royal Academy of Engineering and Canon Medical Research Europe, and partially supported by the Alan Turing Institute under the EPSRC grant EP/N510129/1. S.A. Tsafaris acknowledges the support of Canon Medical and the Royal Academy of Engineering and the Research Chairs and Senior Research Fellowships scheme (grant RCSR1819\8\25). We thank the participants of the DREAM tutorials for feedback.

## REFERENCES

- [1] A. Achille and S. Soatto, "Emergence of Invariance and Disentanglement in Deep Representations," *Journal of Machine Learning Research*, vol. 19, pp. 1–34, 2017.
- [2] B. Schölkopf, F. Locatello, S. Bauer, N. R. Ke, N. Kalchbrenner, A. Goyal, and Y. Bengio, "Toward causal representation learning," *Proceedings of the IEEE*, vol. 109, no. 5, 2021.
- [3] J. Peters, D. Janzing, and B. Schölkopf, *Elements of causal inference: foundations and learning algorithms*. The MIT Press, 2017.
- [4] J. Pearl, *Causality: Models, Reasoning and Inference*, 2nd ed. USA: Cambridge University Press, 2009.
- [5] Y. Bengio, A. Courville, and P. Vincent, "Representation learning: A review and new perspectives," *IEEE Transactions on Pattern Analysis and Machine Intelligence*, vol. 35, no. 8, pp. 1798–1828, 2013.
- [6] I. Higgins, D. Amos, D. Pfau, S. Racaniere, L. Matthey, D. Rezende, and A. Lerchner, "Towards a definition of disentangled representations," *arXiv:1812.02230*, 2018.
- [7] R. C. o. Petersen, "Alzheimer's disease neuroimaging initiative (ADNI)," *Neurology*, vol. 74, no. 3, pp. 201–209, 2010.
- [8] S. E. Reed, Y. Zhang, Y. Zhang, and H. Lee, "Deep visual analogy-making," in *Proc. International Conference on Neural Information Processing Systems (NeurIPS)*, 2015.
- [9] C. Burgess and H. Kim, "3d shapes dataset," <https://github.com/deepmind/3dshapes-dataset/>, 2018.
- [10] V. N. Vapnik, "An overview of statistical learning theory," *IEEE Transactions on Neural Networks*, vol. 10, no. 5, pp. 988–999, 1999.
- [11] M. Leshno, V. Y. Lin, A. Pinkus, and S. Schocken, "Multilayer feedforward networks with a nonpolynomial activation function can approximate any function," *Neural networks*, vol. 6, no. 6, pp. 861–867, 1993.
- [12] T. Cohen and M. Welling, "Group equivariant convolutional networks," in *Proc. International Conference on Machine Learning (ICML)*, 2016, pp. 2990–2999.
- [13] T. Cohen, "Equivariant convolutional networks," Ph.D. dissertation, University of Amsterdam, 2021.
- [14] M. M. Bronstein, J. Bruna, T. Cohen, and P. Veličković, "Geometric deep learning: Grids, groups, graphs, geodesics, and gauges," *arXiv pre-print*, vol. 2104.13478, 2021.
- [15] K. Lenc and A. Vedaldi, "Understanding image representations by measuring their equivariance and equivalence," in *Proc. IEEE/CVF Conference on Computer Vision and Pattern Recognition (CVPR)*, 2015, pp. 991–999.
- [16] A. L. Yuille and C. Liu, "Deep nets: What have they ever done for vision?" *International Journal of Computer Vision*, vol. 129, no. 3, pp. 781–802, 2021.
- [17] J. Pearl and D. Mackenzie, *The Book of Why: The New Science of Cause and Effect*, 1st ed. USA: Basic Books, Inc., 2018.
- [18] H. Caselles-Dupré, M. Garcia Ortiz, and D. Filliat, "Symmetry-based disentangled representation learning requires interaction with environments," in *Proc. International Conference on Neural Information Processing Systems (NeurIPS)*, 2019, pp. 4606–4615.
- [19] M. Besserve, A. Mehrjou, R. Sun, and B. Schölkopf, "Counterfactuals uncover the modular structure of deep generative models," *International Conference on Learning Representations (ICLR)*, 2020.
- [20] D. C. Castro, I. Walker, and B. Glocker, "Causality matters in medical imaging," *Nature Communications*, vol. 11, no. 1, pp. 1–10, 2020.
- [21] F. Locatello, S. Bauer, M. Lucic, G. Raetsch, S. Gelly, B. Schölkopf, and O. Bachem, "Challenging common assumptions in the unsupervised learning of disentangled representations," in *Proc. International Conference on Machine Learning (ICML)*, 2019, pp. 4114–4124.
- [22] V. Thomas, J. Pondard, E. Bengio, M. Sarfati, P. Beaudoin, M.-J. Meurs, J. Pineau, D. Precup, and Y. Bengio, "Independently controllable features," *arXiv:1708.01289*, 2017.
- [23] X. Chen, Y. Duan, R. Houthoofd, J. Schulman, I. Sutskever, and P. Abbeel, "InfoGAN: Interpretable representation learning by information maximizing generative adversarial nets," in *Proc. International Conference on Neural Information Processing Systems (NeurIPS)*, 2016, p. 2180–2188.
- [24] C. Eastwood and C. K. I. Williams, "A framework for the quantitative evaluation of disentangled representations," *International Conference on Learning Representations (ICLR)*, 2018.
- [25] K. Ridgeway and M. C. Mozer, "Learning deep disentangled embeddings with the F-statistic loss," in *Proc.*

- International Conference on Neural Information Processing Systems (NeurIPS)*, 2018, p. 185–194.
- [26] N. Tishby, F. C. Pereira, and W. Bialek, “The information bottleneck method,” in *Proc. Annual Allerton Conference on Communication, Control and Computing*, 1999.
  - [27] I. Higgins, L. Matthey, A. Pal, C. Burgess, X. Glorot, M. Botvinick, S. Mohamed, and A. Lerchner, “ $\beta$ -VAE: Learning basic visual concepts with a constrained variational framework,” *International Conference on Learning Representations (ICLR)*, 2017.
  - [28] R. T. Q. Chen, X. Li, R. B. Grosse, and D. K. Duvenaud, “Isolating sources of disentanglement in variational autoencoders,” in *Proc. International Conference on Neural Information Processing Systems (NeurIPS)*, 2018.
  - [29] H. Kim and A. Mnih, “Disentangling by factorising,” in *Proc. International Conference on Machine Learning (ICML)*, 2018, pp. 2649–2658.
  - [30] I. Khemakhem, D. Kingma, R. Monti, and A. Hyvärinen, “Variational autoencoders and nonlinear ICA: A unifying framework,” in *Proc. International Conference on Artificial Intelligence and Statistics (AISTATS)*, vol. 108, 2020, pp. 2207–2217.
  - [31] A. Hyvärinen and P. Pajunen, “Nonlinear independent component analysis: Existence and uniqueness results,” *Neural networks*, vol. 12, no. 3, pp. 429–439, 1999.
  - [32] Y. Lecun, L. Bottou, Y. Bengio, and P. Haffner, “Gradient-based learning applied to document recognition,” *Proceedings of the IEEE*, vol. 86, no. 11, pp. 2278–2324, 1998.
  - [33] A. Graves, A.-r. Mohamed, and G. Hinton, “Speech recognition with deep recurrent neural networks,” in *Proc. of IEEE international conference on acoustics, speech and signal processing*, 2013, pp. 6645–6649.
  - [34] Y. LeCun, Y. Bengio, and G. Hinton, “Deep learning,” *Nature*, vol. 521, no. 7553, pp. 436–444, 2015.
  - [35] A. Vaswani, N. Shazeer, N. Parmar, J. Uszkoreit, L. Jones, A. N. Gomez, u. Kaiser, and I. Polosukhin, “Attention is all you need,” in *Proc. International Conference on Neural Information Processing Systems (NeurIPS)*, 2017.
  - [36] D. P. Kingma and M. Welling, “Auto-encoding variational bayes,” *International Conference on Learning Representations (ICLR)*, 2014.
  - [37] D. J. Rezende, S. Mohamed, and D. Wierstra, “Stochastic backpropagation and approximate inference in deep generative models,” in *Proc. International Conference on Machine Learning (ICML)*, 2014, pp. 1278–1286.
  - [38] B. Cheung, J. A. Livezey, A. K. Bansal, and B. A. Olshausen, “Discovering hidden factors of variation in deep networks,” *International Conference on Learning Representations Workshop (ICLRW)*, 2015.
  - [39] S. N. B. Paige, J.-W. van de Meent, A. Desmaison, N. Goodman, P. Kohli, F. Wood, and P. Torr, “Learning disentangled representations with semi-supervised deep generative models,” in *Proc. International Conference on Neural Information Processing Systems (NeurIPS)*, 2017.
  - [40] S. Watanabe, “Information theoretical analysis of multivariate correlation,” *IBM Journal of research and development*, vol. 4, no. 1, pp. 66–82, 1960.
  - [41] M. Rolinek, D. Zietlow, and G. Martius, “Variational autoencoders pursue PCA directions (by accident),” in *Proc. IEEE/CVF Conference on Computer Vision and Pattern Recognition (CVPR)*, 2019, pp. 12 406–12 415.
  - [42] C. P. Burgess, I. Higgins, A. Pal, L. Matthey, N. Waters, G. Desjardins, and A. Lerchner, “Understanding disentangling in  $\beta$ -vae,” *arXiv:1804.03599*, 2018.
  - [43] B. Esmaeili, H. Wu, S. Jain, A. Bozkurt, N. Siddharth, B. Paige, D. H. Brooks, J. Dy, and J. van de Meent, “Structured disentangled representations,” in *Proc. International Conference on Artificial Intelligence and Statistics (AISTATS)*, 2019, pp. 2525–2534.
  - [44] I. Goodfellow, J. Pouget-Abadie, M. Mirza, B. Xu, D. Warde-Farley, S. Ozair, A. Courville, and Y. Bengio, “Generative adversarial nets,” in *Proc. International Conference on Neural Information Processing Systems (NeurIPS)*, 2014.
  - [45] T. Karras, S. Laine, and T. Aila, “A style-based generator architecture for generative adversarial networks,” in *Proc. IEEE/CVF Conference on Computer Vision and Pattern Recognition (CVPR)*, 2019, pp. 4401–4410.
  - [46] A. Brock, J. Donahue, and K. Simonyan, “Large scale GAN training for high fidelity natural image synthesis,” *International Conference on Learning Representations Workshop (ICLR)*, 2019.
  - [47] B. Liu, Y. Zhu, Z. Fu, G. de Melo, and A. Elgammal, “OOGAN: Disentangling GAN with one-hot sampling and orthogonal regularization,” in *Proc. AAAI Conference on Artificial Intelligence (AAAI)*, 2020, pp. 4836–4843.
  - [48] Y. Shen and B. Zhou, “Closed-form factorization of latent semantics in GANs,” in *Proc. IEEE/CVF Conference on Computer Vision and Pattern Recognition (CVPR)*, 2021, pp. 1532–1540.
  - [49] S. Mukherjee, H. Asnani, E. Lin, and S. Kannan, “ClusterGAN: Latent space clustering in generative adversarial networks,” in *Proc. AAAI Conference on Artificial Intelligence (AAAI)*, 2019, pp. 4610–4617.
  - [50] T. Karras, S. Laine, M. Aittala, J. Hellsten, J. Lehtinen, and T. Aila, “Analyzing and improving the image quality of StyleGAN,” in *Proc. IEEE/CVF Conference on Computer Vision and Pattern Recognition (CVPR)*, 2020, pp. 8107–8116.
  - [51] W. Nie, T. Karras, A. Garg, S. Debnath, A. Patney, A. Patel, and A. Anandkumar, “Semi-supervised StyleGAN for disentanglement learning,” in *Proc. International Conference on Machine Learning (ICML)*, 2020, pp. 7360–7369.
  - [52] W. Peebles, J. Peebles, J.-Y. Zhu, A. A. Efros, and A. Torralba, “The hessian penalty: A weak prior for unsupervised disentanglement,” in *Proc. European Conference on Computer Vision (ECCV)*, 2020, pp. 581–597.
  - [53] L. Dinh, D. Krueger, and Y. Bengio, “Nice: Non-linear independent components estimation,” in *International Conference on Learning Representations Workshops (ICLRW)*, 2015.
  - [54] D. Rezende and S. Mohamed, “Variational inference with normalizing flows,” in *Proc. International Conference on Machine Learning (ICML)*, 2015, pp. 1530–1538.

- [55] D. P. Kingma and P. Dhariwal, "Glow: Generative flow with invertible 1x1 convolutions," in *Proc. International Conference on Neural Information Processing Systems (NeurIPS)*, 2018.
- [56] G. Papamakarios, E. Nalisnick, D. J. Rezende, S. Mohamed, and B. Lakshminarayanan, "Normalizing flows for probabilistic modeling and inference," *Journal of Machine Learning Research*, vol. 22, pp. 1–64, 2021.
- [57] P. Esser, R. Rombach, and B. Ommer, "A disentangling invertible interpretation network for explaining latent representations," in *Proc. IEEE/CVF Conference on Computer Vision and Pattern Recognition (CVPR)*, 2020, pp. 9223–9232.
- [58] A. Sankar, M. Keicher, R. Eisawy, A. Parida, F. Pfister, S. T. Kim, and N. Navab, "GLOWin: A flow-based invertible generative framework for learning disentangled feature representations in medical images," *arXiv:2103.10868*, 2021.
- [59] I. Kobyzev, S. Prince, and M. Brubaker, "Normalizing flows: An introduction and review of current methods," *IEEE Transactions on Pattern Analysis and Machine Intelligence (Early Access)*, 2020.
- [60] L. A. Gatys, A. S. Ecker, and M. Bethge, "Image style transfer using convolutional neural networks," in *Proc. IEEE/CVF Conference on Computer Vision and Pattern Recognition (CVPR)*, 2016, pp. 2414–2423.
- [61] A. Gabbay and Y. Hoshen, "Demystifying inter-class disentanglement," *International Conference on Learning Representations (ICLR)*, 2020.
- [62] D. Ruta, S. Motiian, B. Faieta, Z. Lin, H. Jin, A. Filipkowski, A. Gilbert, and J. Collomosse, "ALADIN: All layer adaptive instance normalization for fine-grained style similarity," *arXiv:2103.09776*, 2021.
- [63] X. Huang, M.-Y. Liu, S. Belongie, and J. Kautz, "Multimodal unsupervised image-to-image translation," in *Proc. European Conference on Computer Vision (ECCV)*, 2018, pp. 172–189.
- [64] H.-Y. Lee, H.-Y. Tseng, J.-B. Huang, M. K. Singh, and M.-H. Yang, "Diverse image-to-image translation via disentangled representations," in *Proc. European Conference on Computer Vision (ECCV)*, 2018, pp. 36–52.
- [65] A. Chartsias, T. Joyce, G. Papanastasiou, S. Semple, M. Williams, D. E. Newby, R. Dharmakumar, and S. A. Tsaftaris, "Disentangled representation learning in cardiac image analysis," *Medical Image Analysis*, vol. 58, p. 101535, 2019.
- [66] D. Ulyanov, A. Vedaldi, and V. Lempitsky, "Improved texture networks: Maximizing quality and diversity in feed-forward stylization and texture synthesis," in *Proc. IEEE/CVF Conference on Computer Vision and Pattern Recognition (CVPR)*, 2017, pp. 4105–4113.
- [67] X. Huang and S. Belongie, "Arbitrary style transfer in real-time with adaptive instance normalization," in *Proc. IEEE/CVF International Conference on Computer Vision (ICCV)*, 2017, pp. 1501–1510.
- [68] S. Ioffe and C. Szegedy, "Batch normalization: Accelerating deep network training by reducing internal covariate shift," in *Proc. International Conference on Machine Learning (ICML)*, 2015, pp. 448–456.
- [69] Q. Liu, C. Chen, J. Qin, Q. Dou, and P.-A. Heng, "FedDG: Federated domain generalization on medical image segmentation via episodic learning in continuous frequency space," in *Proc. IEEE/CVF Conference on Computer Vision and Pattern Recognition (CVPR)*, 2021, pp. 1013–1023.
- [70] J. Huang, D. Guan, A. Xiao, and S. Lu, "FSDR: Frequency space domain randomization for domain generalization," in *Proc. IEEE/CVF Conference on Computer Vision and Pattern Recognition (CVPR)*, 2021, pp. 6891–6902.
- [71] E. Perez, F. Strub, H. de Vries, V. Dumoulin, and A. C. Courville, "FiLM: Visual reasoning with a general conditioning layer," in *Proc. AAAI Conference on Artificial Intelligence (AAAI)*, 2018, pp. 3942–3951.
- [72] T. Park, M.-Y. Liu, T.-C. Wang, and J.-Y. Zhu, "Semantic image synthesis with spatially-adaptive normalization," in *Proc. IEEE/CVF Conference on Computer Vision and Pattern Recognition (CVPR)*, 2019, pp. 2337–2346.
- [73] Y. Ganin and V. Lempitsky, "Unsupervised domain adaptation by backpropagation," in *Proc. International Conference on Machine Learning*, 2015, pp. 1180–1189.
- [74] A. Gonzalez-Garcia, J. Van De Weijer, and Y. Bengio, "Image-to-image translation for cross-domain disentanglement," *arXiv:1805.09730*, 2018.
- [75] P. Esser, E. Sutter, and B. Ommer, "A variational U-Net for conditional appearance and shape generation," in *Proc. IEEE/CVF Conference on Computer Vision and Pattern Recognition (CVPR)*, 2018, pp. 8857–8866.
- [76] D. Lorenz, L. Bereska, T. Milbich, and B. Ommer, "Unsupervised part-based disentanglement of object shape and appearance," in *Proc. IEEE/CVF Conference on Computer Vision and Pattern Recognition (CVPR)*, 2019, pp. 10955–10964.
- [77] J.-Y. Zhu, T. Park, P. Isola, and A. A. Efros, "Unpaired image-to-image translation using cycle-consistent adversarial networks," in *Proc. IEEE/CVF International Conference on Computer Vision*, 2017, pp. 2223–2232.
- [78] A. Almahairi, S. Rajeshwar, A. Sordoni, P. Bachman, and A. Courville, "Augmented CycleGAN: Learning many-to-many mappings from unpaired data," in *Proc. International Conference on Machine Learning (ICML)*, 2018, pp. 195–204.
- [79] Y. Hiasa, Y. Otake, M. Takao, T. Matsuoka, K. Takashima, A. Carass, J. L. Prince, N. Sugano, and Y. Sato, "Cross-modality image synthesis from unpaired data using CycleGAN," in *Proc. International Workshop on Simulation and Synthesis in Medical Imaging (SASHIMI)*, 2018, pp. 31–41.
- [80] R. Zhang, T. Pfister, and J. Li, "Harmonic unpaired image-to-image translation," *International Conference on Learning Representations (ICLR)*, 2019.
- [81] T. Xia, A. Chartsias, S. A. Tsaftaris, A. D. N. Initiative et al., "Consistent brain ageing synthesis," in *Proc. International Conference on Medical Image Computing and Computer-Assisted Intervention (MICCAI)*, 2019, pp. 750–758.
- [82] T. Xia, A. Chartsias, and S. A. Tsaftaris, "Pseudo-healthy synthesis with pathology disentanglement and adversarial learning," *Medical Image Analysis*, vol. 64, p. 101719, 2020.
- [83] C. Li, H. Liu, C. Chen, Y. Pu, L. Chen, R. Henao, and L. Carin, "ALICE: Towards understanding adversarial

- learning for joint distribution matching," in *Proc. International Conference on Neural Information Processing Systems (NeurIPS)*, 2017.
- [84] A. Jahanian, L. Chai, and P. Isola, "On the "steerability" of generative adversarial networks," *International Conference on Learning Representations Workshop (ICLR)*, 2020.
- [85] A. Cherepkov, A. Voynov, and A. Babenko, "Navigating the GAN parameter space for semantic image editing," in *Proc. IEEE/CVF Conference on Computer Vision and Pattern Recognition (CVPR)*, 2021.
- [86] A. Kumar, P. Sattigeri, and A. Balakrishnan, "Variational inference of disentangled latent concepts from unlabeled observations," *International Conference on Learning Representations (ICLR)*, 2018.
- [87] J. Zaidi, J. Boilard, G. Gagnon, and M.-A. Carboneau, "Measuring disentanglement: A review of metrics," *arXiv:2012.09276*, 2020.
- [88] X. Liu, S. Thermos, G. Valvano, A. Chartsias, A. O'Neil, and S. A. Tsaftaris, "Metrics for exposing the biases of content-style disentanglement," *arXiv:2008.12378*, 2020.
- [89] G. J. Székely, M. L. Rizzo, N. K. Bakirov *et al.*, "Measuring and testing dependence by correlation of distances," *The Annals of Statistics*, vol. 35, no. 6, pp. 2769–2794, 2007.
- [90] N. Cristianini, J. Shawe-Taylor, A. Elisseeff, and J. S. Kandola, "On kernel-target alignment," in *Proc. Advances in Neural Information Processing Systems (NeurIPS)*, 2002, pp. 367–373.
- [91] A. Gretton, O. Bousquet, A. Smola, and B. Schölkopf, "Measuring statistical dependence with hilbertschmidt norms," in *Proc. of International Conference on algorithmic learning theory*, 2005, pp. 63–77.
- [92] J.-Y. Zhu, R. Zhang, D. Pathak, T. Darrell, A. A. Efros, O. Wang, and E. Shechtman, "Toward multi-modal image-to-image translation," in *Proc. International Conference on Neural Information Processing Systems (NeurIPS)*, 2017, pp. 465–476.
- [93] G. Ros, L. Sellart, J. Materzynska, D. Vazquez, and A. M. Lopez, "The SYNTHIA dataset: A large collection of synthetic images for semantic segmentation of urban scenes," in *Proc. IEEE/CVF Conference on Computer Vision and Pattern Recognition (CVPR)*, 2016, pp. 3234–3243.
- [94] M. Cordts, M. Omran, S. Ramos, T. Rehfeld, M. Enzweiler, R. Benenson, U. Franke, S. Roth, and B. Schiele, "The Cityscapes dataset for semantic urban scene understanding," in *Proc. IEEE/CVF Conference on Computer Vision and Pattern Recognition (CVPR)*, 2016, pp. 3213–3223.
- [95] J.-Y. Zhu, P. Krähenbühl, E. Shechtman, and A. A. Efros, "Generative visual manipulation on the natural image manifold," in *Proc. European Conference on Computer Vision (ECCV)*, 2016, pp. 597–613.
- [96] J.-Y. Zhu, T. Park, P. Isola, and A. A. Efros, "Unpaired image-to-image translation using cycle-consistent adversarial networks," in *Proc. IEEE/CVF International Conference on Computer Vision (ICCV)*, 2017, pp. 2223–2232.
- [97] H.-Y. Lee, H.-Y. Tseng, J.-B. Huang, M. Singh, and M.-H. Yang, "Diverse image-to-image translation via disentangled representations," in *Proc. European Conference on Computer Vision (ECCV)*, 2018, pp. 36–52.
- [98] J. Lin, Y. Xia, T. Qin, Z. Chen, and T.-Y. Liu, "Conditional image-to-image translation," in *Proc. IEEE/CVF Conference on Computer Vision and Pattern Recognition (CVPR)*, 2018, pp. 5524–5532.
- [99] W. Wu, K. Cao, C. Li, C. Qian, and C. C. Loy, "TransGaGa: Geometry-aware unsupervised image-to-image translation," *Proc. IEEE/CVF Conference on Computer Vision and Pattern Recognition*, pp. 8004–8013, 2019.
- [100] T. Park, A. A. Efros, R. Zhang, and J.-Y. Zhu, "Contrastive learning for unpaired image-to-image translation," in *Proc. European Conference on Computer Vision (ECCV)*, 2020, pp. 319–345.
- [101] T. Xiao, J. Hong, and J. Ma, "ELEGANT: Exchanging latent encodings with GAN for transferring multiple face attributes," in *Proc. European Conference on Computer Vision (ECCV)*, 2018, pp. 172–187.
- [102] O. Ronneberger, P. Fischer, and T. Brox, "U-Net: Convolutional networks for biomedical image segmentation," in *Proc. International Conference on Medical Image Computing and Computer-Assisted Intervention (MICCAI)*, 2015, pp. 234–241.
- [103] J. Lin, Z. Chen, Y. Xia, S. Liu, T. Qin, and J. Luo, "Exploring explicit domain supervision for latent space disentanglement in unpaired image-to-image translation," *IEEE Transactions on Pattern Analysis and Machine Intelligence*, vol. 43, no. 4, pp. 1254–1266, 2021.
- [104] Z. He, W. Zuo, M. Kan, S. Shan, and X. Chen, "AttGAN: Facial attribute editing by only changing what you want," *IEEE Transactions on Image Processing*, vol. 28, no. 11, pp. 5464–5478, 2019.
- [105] S. Zhou, T. Xiao, Y. Yang, D. Feng, Q. He, and W. He, "GeneGAN: Learning object transfiguration and attribute subspace from unpaired data," in *Proc. British Machine Vision Conference (BMVC)*, 2017.
- [106] C. Ionescu, D. Papava, V. Olaru, and C. Sminchisescu, "Human3.6M: Large scale datasets and predictive methods for 3D human sensing in natural environments," *IEEE Transactions on Pattern Analysis and Machine Intelligence*, vol. 36, no. 7, pp. 1325–1339, 2014.
- [107] W. Zhang, M. Zhu, and K. G. Derpanis, "From actemes to action: A strongly-supervised representation for detailed action understanding," in *Proc. IEEE/CVF International Conference on Computer Vision (ICCV)*, 2013, pp. 2248–2255.
- [108] P. Esser, J. Haux, and B. Ommer, "Unsupervised robust disentangling of latent characteristics for image synthesis," in *Proc. IEEE/CVF International Conference on Computer Vision (ICCV)*, 2019, pp. 2699–2709.
- [109] J. Kim, J. Yoo, J. Lee, and S. Hong, "SetVAE: Learning hierarchical composition for generative modeling of set-structured data," in *Proc. IEEE/CVF Conference on Computer Vision and Pattern Recognition (CVPR)*, 2021, pp. 15 059–15 068.
- [110] C. K. Sønderby, T. Raiko, L. Maaløe, S. K. Sønderby, and O. Winther, "Ladder variational autoencoders," in *Proc. International Conference on Neural Information Processing Systems (NeurIPS)*, 2016, p. 3745–3753.

- [111] A. Vahdat and J. Kautz, "NVAE: A deep hierarchical variational autoencoder," in *Proc. International Conference on Neural Information Processing Systems (NeurIPS)*, 2020.
- [112] J. Lee, Y. Lee, J. Kim, A. Kosiorrek, S. Choi, and Y. W. Teh, "Set Transformer: A framework for attention-based permutation-invariant neural networks," in *Proc. International Conference on Machine Learning (ICML)*, 2019, pp. 3744–3753.
- [113] A. X. Chang *et al.*, "ShapeNet: An information-rich 3D model repository," *Technical report*, 2015.
- [114] Y. Zhang, J. Hare, and A. Prügel-Bennett, "Deep Set Prediction Networks," in *Proc. International Conference on Neural Information Processing Systems (NeurIPS)*, 2019.
- [115] S. M. A. Eslami, N. Heess, T. Weber, Y. Tassa, D. Szepesvari, K. Kavukcuoglu, and G. E. Hinton, "Attend, infer, repeat: Fast scene understanding with generative models," in *Proc. International Conference on Neural Information Processing Systems (NeurIPS)*, 2016, p. 3233–3241.
- [116] F. Locatello, D. Weissenborn, T. Unterthiner, A. Mahendran, G. Heigold, J. Uszkoreit, A. Dosovitskiy, and T. Kipf, "Object-centric learning with slot attention," in *Proc. International Conference on Neural Information Processing Systems (NeurIPS)*, 2020.
- [117] G. Yang, X. Huang, Z. Hao, M.-Y. Liu, S. Belongie, and B. Hariharan, "PointFlow: 3D point cloud generation with continuous normalizing flows," in *Proc. IEEE/CVF International Conference on Computer Vision (ICCV)*, 2019, pp. 4541–4550.
- [118] Y. Bengio, N. Léonard, and A. Courville, "Estimating or propagating gradients through stochastic neurons for conditional computation," *arXiv:1308.3432*, 2013.
- [119] O. Bernard *et al.*, "Deep learning techniques for automatic MRI cardiac multi-structures segmentation and diagnosis: Is the problem solved?" *IEEE Transactions on Medical Imaging*, vol. 37, no. 11, pp. 2514–2525, 2018.
- [120] X. Zhuang and J. Shen, "Multi-scale patch and multi-modality atlases for whole heart segmentation of mri," *Medical Image Analysis*, vol. 31, pp. 77–87, 2016.
- [121] X. Zhuang, "Challenges and methodologies of fully automatic whole heart segmentation: A review," *Journal of Healthcare Engineering*, vol. 4, no. 3, pp. 371–407, 2013.
- [122] X. Zhuang, K. S. Rhode, R. S. Razavi, D. J. Hawkes, and S. Ourselin, "A registration-based propagation framework for automatic whole heart segmentation of cardiac MRI," *IEEE Transactions on Medical Imaging*, vol. 29, no. 9, pp. 1612–1625, 2010.
- [123] V. M. Campello *et al.*, "Multi-centre, multi-vendor and multi-disease cardiac segmentation: The M&Ms challenge," *IEEE Transactions on Medical Imaging (Early Access)*, 2021.
- [124] F. Prados, J. Ashburner, C. Blaiotta, T. Brosch, J. Carballido-Gamio, M. J. Cardoso, B. N. Conrad, E. Datta, G. David, B. De Leener *et al.*, "Spinal cord grey matter segmentation challenge," *Neuroimage*, vol. 152, pp. 312–329, 2017.
- [125] X. Liu, S. Thermos, A. Chatsias, A. O'Neil, and S. A. Tsafaris, "Disentangled representations for domain-generalized cardiac segmentation," in *Proc. International Workshop on Statistical Atlases and Computational Models of the Heart (STACOM)*, 2020, pp. 187–195.
- [126] S. Thermos, X. Liu, A. O'Neil, and S. A. Tsafaris, "Controllable cardiac synthesis via disentangled anatomy arithmetic," in *Proc. International Conference on Medical Image Computing and Computer-Assisted Intervention (MICCAI)*, 2021.
- [127] E. Jang, S. Gu, and B. Poole, "Categorical reparameterization with Gumbel-softmax," *arXiv:1611.01144*, 2016.
- [128] G. Valvano, A. Chatsias, A. Leo, and S. A. Tsafaris, "Temporal consistency objectives regularize the learning of disentangled representations," in *Proc. MICCAI Workshop on Domain Adaptation and Representation Transfer (DART)*, 2019, pp. 11–19.
- [129] X. Liu, S. Thermos, A. O'Neil, and S. A. Tsafaris, "Semi-supervised meta-learning with disentanglement for domain-generalised medical image segmentation," in *Proc. International Conference on Medical Image Computing and Computer-Assisted Intervention (MICCAI)*, 2021.
- [130] C. I. Bercea, B. Wiestler, D. Rueckert, and S. Albarqouni, "FedDis: Disentangled federated learning for unsupervised brain pathology segmentation," *arXiv:2103.03705*, 2021.
- [131] D. Li, J. Yang, K. Kreis, A. Torralba, and S. Fidler, "Semantic segmentation with generative models: Semi-supervised learning and strong out-of-domain generalization," in *Proc. IEEE/CVF Conference on Computer Vision and Pattern Recognition (CVPR)*, 2021, pp. 8300–8311.
- [132] J. Yang, X. Li, D. Pak, N. C. Dvornek, J. Chapiro, M. Lin, and J. S. Duncan, "Cross-modality segmentation by self-supervised semantic alignment in disentangled content space," in *Proc. MICCAI Workshop on Domain Adaptation and Representation Transfer (DART)*, 2020, pp. 52–61.
- [133] J. Yang, N. C. Dvornek, F. Zhang, J. Chapiro, M. Lin, and J. S. Duncan, "Unsupervised domain adaptation via disentangled representations: Application to cross-modality liver segmentation," in *Proc. International Conference on Medical Image Computing and Computer-Assisted Intervention (MICCAI)*, 2019, pp. 255–263.
- [134] C. Pei, F. Wu, L. Huang, and X. Zhuang, "Disentangle domain features for cross-modality cardiac image segmentation," *Medical Image Analysis*, vol. 71, p. 102078, 2021.
- [135] C. Chen, Q. Dou, Y. Jin, H. Chen, J. Qin, and P.-A. Heng, "Robust multimodal brain tumor segmentation via feature disentanglement and gated fusion," in *Proc. International Conference on Medical Image Computing and Computer-Assisted Intervention (MICCAI)*, 2019, pp. 447–456.
- [136] J. Ouyang, E. Adeli, K. M. Pohl, Q. Zhao, and G. Zaharchuk, "Representation disentanglement for multi-modal MR analysis," *arXiv:2102.11456*, 2021.
- [137] C. Chen, C. Ouyang, G. Tarroni, J. Schlemper, H. Qiu, W. Bai, and D. Rueckert, "Unsupervised multi-modal style transfer for cardiac MR segmentation," in *Proc. International Workshop on Statistical Atlases and Compu-*



- tational Models of the Heart (STACOM)*, 2019, pp. 209–219.
- [138] J. Jiang and H. Veeraraghavan, “Unified cross-modality feature disentangler for unsupervised multi-domain mri abdomen organs segmentation,” in *Proc. International Conference on Medical Image Computing and Computer-Assisted Intervention (MICCAI)*, 2020, pp. 347–358.
- [139] P. Christ, F. Ettlinger, F. Grün, J. Lipkova, and G. Kaissis, “Lits-liver tumor segmentation challenge,” *ISBI and MICCAI*, 2017.
- [140] Q. Zhao, E. V. Sullivan, N. Honnorat, E. Adeli, S. Podhajsky, M. D. De Bellis, J. Voyvodic, K. B. Nooner, F. C. Baker, I. M. Colrain *et al.*, “Association of heavy drinking with deviant fiber tract development in frontal brain systems in adolescents,” *JAMA psychiatry*, vol. 78, no. 4, pp. 407–415, 2021.
- [141] B. H. Menze *et al.*, “The multimodal brain tumor image segmentation benchmark (BRATS),” *IEEE Transactions on Medical Imaging*, vol. 34, no. 10, pp. 1993–2024, 2015.
- [142] A. E. Kavur, N. S. Gezer, M. Barış, S. Aslan, P.-H. Conze, V. Groza, D. D. Pham, S. Chatterjee, P. Ernst, S. Özkan *et al.*, “CHAOS challenge-combined (CT-MR) healthy abdominal organ segmentation,” *Medical Image Analysis*, vol. 69, p. 101950, 2021.
- [143] X. Zhuang, “Multivariate mixture model for cardiac segmentation from multi-sequence mri,” in *Proc. International Conference on Medical Image Computing and Computer-Assisted Intervention (MICCAI)*, 2016, pp. 581–588.
- [144] —, “Multivariate mixture model for myocardial segmentation combining multi-source images,” *IEEE Transactions on Pattern Analysis and Machine Intelligence*, vol. 41, no. 12, pp. 2933–2946, 2019.
- [145] J. Hoffman, E. Tzeng, T. Park, J.-Y. Zhu, P. Isola, K. Saenko, A. Efros, and T. Darrell, “CyCADA: Cycle-consistent adversarial domain adaptation,” in *Proc. International Conference on Machine Learning (ICML)*, 2018, pp. 1989–1998.
- [146] A. Chatsias, G. Papanastasiou, C. Wang, S. Semple, D. E. Newby, R. Dharmakumar, and S. A. Tsaftaris, “Disentangle, align and fuse for multimodal and semi-supervised image segmentation,” *IEEE Transactions on Medical Imaging*, vol. 40, no. 3, pp. 781–792, 2021.
- [147] Y. Lyu, H. Liao, H. Zhu, and S. K. Zhou, “Joint unsupervised learning for the vertebra segmentation, artifact reduction and modality translation of CBCT images,” *arXiv:2001.00339*, 2020.
- [148] K. Kobayashi, R. Hataya, Y. Kurose, M. Miyake, M. Takahashi, A. Nakagawa, T. Harada, and R. Hamamoto, “Decomposing normal and abnormal features of medical images into discrete latent codes for content-based image retrieval,” *arXiv:2103.12328*, 2021.
- [149] O. Maier *et al.*, “ISLES 2015 - A public evaluation benchmark for ischemic stroke lesion segmentation from multispectral MRI,” *Medical Image Analysis*, vol. 35, pp. 250–269, 2017.
- [150] J. R. Taylor, N. Williams, R. Cusack, T. Auer, M. A. Shafto, M. Dixon, L. K. Tyler, Cam-CAN, and R. N. Henson, “The Cambridge centre for ageing and neuroscience (Cam-CAN) data repository: Structural and functional MRI, MEG, and cognitive data from a cross-sectional adult lifespan sample,” *NeuroImage*, vol. 144, pp. 262–269, 2017.
- [151] I. Gulrajani, F. Ahmed, M. Arjovsky, V. Dumoulin, and A. Courville, “Improved training of wasserstein GANs,” in *Proc. International Conference on Neural Information Processing Systems (NeurIPS)*, 2017, p. 5769–5779.
- [152] X. Mao, Q. Li, H. Xie, R. Y. Lau, Z. Wang, and S. P. Smolley, “Least squares generative adversarial networks,” in *Proc. IEEE/CVF International Conference on Computer Vision (ICCV)*, 2017, pp. 2813–2821.
- [153] H. Liao, W.-A. Lin, S. K. Zhou, and J. Luo, “ADN: Artifact disentanglement network for unsupervised metal artifact reduction,” *IEEE Transactions on Medical Imaging*, vol. 39, no. 3, pp. 634–643, 2020.
- [154] Y. Huang, W. Xia, Z. Lu, Y. Liu, J. Zhou, L. Fang, and Y. Zhang, “Disentanglement network for unsupervised speckle reduction of optical coherence tomography images,” in *Proc. International Conference on Medical Image Computing and Computer-Assisted Intervention (MICCAI)*, 2020, pp. 675–684.
- [155] A. Chatsias, T. Joyce, M. V. Giuffrida, and S. A. Tsaftaris, “Multimodal MR synthesis via modality-invariant latent representation,” *IEEE Transactions on Medical Imaging*, vol. 37, no. 3, pp. 803–814, 2018.
- [156] K. Li, L. Yu, S. Wang, and P.-A. Heng, “Unsupervised retina image synthesis via disentangled representation learning,” in *Proc. International Workshop on Simulation and Synthesis in Medical Imaging (SASHIMI)*, 2019, pp. 32–41.
- [157] T. Zhou, H. Fu, G. Chen, J. Shen, and L. Shao, “Hi-Net: Hybrid-fusion network for multi-modal MR image synthesis,” *IEEE Transactions on Medical Imaging*, vol. 39, no. 9, pp. 2772–2781, 2020.
- [158] Y. Tang, Y. Tang, Y. Zhu, J. Xiao, and R. M. Summers, “A disentangled generative model for disease decomposition in chest X-rays via normal image synthesis,” *Medical Image Analysis*, vol. 67, p. 101839, 2021.
- [159] T. Xia, A. Chatsias, and S. A. Tsaftaris, “Adversarial pseudo healthy synthesis needs pathology factorization,” in *Proc. International Conference on Medical Imaging with Deep Learning (MIDL)*, 2019, pp. 512–526.
- [160] K. Schutte, O. Moindrot, P. Hérent, J.-B. Schiratti, and S. Jégou, “Using StyleGAN for visual interpretability of deep learning models on medical images,” *arXiv:2101.07563*, 2021.
- [161] T. Joyce, A. Chatsias, and S. A. Tsaftaris, “Robust multi-modal mr image synthesis,” in *Proc. International Conference on Medical Image Computing and Computer-Assisted Intervention (MICCAI)*, 2017, pp. 347–355.
- [162] S. Liu, E. Gibson, S. Grbic, Z. Xu, A. A. A. Setio, J. Yang, B. Georgescu, and D. Comaniciu, “Decompose to manipulate: Manipulable object synthesis in 3D medical images with structured image decomposition,” *arXiv:1812.01737*, 2018.
- [163] M. Pfeiffer *et al.*, “Generating large labeled data sets for laparoscopic image processing tasks using un-

- paired image-to-image translation," in *Proc. Medical Image Computing and Computer Assisted Intervention (MICCAI)*, 2019, pp. 119–127.
- [164] M. Havaei, X. Mao, Y. Wang, and Q. Lao, "Conditional generation of medical images via disentangled adversarial inference," *Medical Image Analysis*, vol. 72, p. 102106, 2021.
- [165] B. E. Dewey *et al.*, "A disentangled latent space for cross-site mri harmonization," in *Proc. International Conference on Medical Image Computing and Computer-Assisted Intervention (MICCAI)*, 2020, pp. 720–729.
- [166] L. Zuo, B. E. Dewey, A. Carass, Y. Liu, Y. He, P. A. Calabresi, and J. L. Prince, "Information-based disentangled representation learning for unsupervised MR harmonization," *arXiv:2103.13283*, 2021.
- [167] N. Pawlowski, D. C. Castro, and B. Glocker, "Deep structural causal models for tractable counterfactual inference," in *Proc. International Conference on Neural Information Processing Systems (NeurIPS)*, 2020.
- [168] J. C. Reinhold, A. Carass, and J. L. Prince, "A structural causal model for MR images of multiple sclerosis," *arXiv:2103.03158*, 2021.
- [169] C. Sudlow *et al.*, "Uk biobank: An open access resource for identifying the causes of a wide range of complex diseases of middle and old age," *Plos med*, vol. 12, no. 3, p. e1001779, 2015.
- [170] C. Durkan, A. Bekasov, I. Murray, and G. Papamakarios, "Neural spline flows," in *Proc. International Conference on Neural Information Processing Systems (NeurIPS)*, 2019.
- [171] E. Bingham, J. P. Chen, M. Jankowiak, F. Obermeyer, N. Pradhan, T. Karaletsos, R. Singh, P. Szerlip, P. Horsfall, and N. D. Goodman, "Pyro: Deep universal probabilistic programming," *The Journal of Machine Learning Research (JMLR)*, vol. 20, no. 1, pp. 973–978, 2019.
- [172] M. Kocaoglu, C. Snyder, A. G. Dimakis, and S. Vishwanath, "CausalGAN: Learning causal implicit generative models with adversarial training," *International Conference on Learning Representations (ICLR)*, 2018.
- [173] H. M. Dolatabadi, S. Erfani, and C. Leckie, "Invertible generative modeling using linear rational splines," in *Proc. International Conference on Artificial Intelligence and Statistics (AISTATS)*, 2020, pp. 4236–4246.
- [174] A. Ben-Cohen, R. Mechrez, N. Yedidia, and H. Greenspan, "Improving CNN training using disentanglement for liver lesion classification in CT," in *Proc. IEEE Engineering in Medicine and Biology Society (EMBC)*, 2019, pp. 886–889.
- [175] Q. Meng, N. Pawlowski, D. Rueckert, and B. Kainz, "Representation disentanglement for multi-task learning with application to fetal ultrasound," in *Proc. Smart Ultrasound Imaging and Perinatal, Preterm and Paediatric Image Analysis (PIPPI)*, 2019, pp. 47–55.
- [176] Q. Meng, J. Matthew, V. A. Zimmer, A. Gomez, D. F. A. Lloyd, D. Rueckert, and B. Kainz, "Mutual information-based disentangled neural networks for classifying unseen categories in different domains: Application to fetal ultrasound imaging," *IEEE Transactions on Medical Imaging*, vol. 40, no. 2, pp. 722–734, 2021.
- [177] M. I. Belghazi, A. Baratin, S. Rajeshwar, S. Ozair, Y. Bengio, A. Courville, and D. Hjelm, "Mutual information neural estimation," in *Proc. International Conference on Machine Learning (ICML)*, 2018, pp. 531–540.
- [178] D. Berthelot, N. Carlini, I. Goodfellow, N. Papernot, A. Oliver, and C. A. Raffel, "Mixmatch: A holistic approach to semi-supervised learning," in *Proc. of Advances in Neural Information Processing Systems (NeurIPS)*, 2019.
- [179] Q. Zhao, E. Adeli, N. Honnorat, T. Leng, and K. M. Pohl, "Variational autoEncoder for regression: Application to brain aging analysis," in *Proc. International Conference on Medical Image Computing and Computer-Assisted Intervention (MICCAI)*, 2019, p. 823–831.
- [180] A. D. Berenguer *et al.*, "Explainable-by-design semi-supervised representation learning for COVID-19 diagnosis from CT imaging," *arXiv:2011.11719*, 2020.
- [181] Q. Zhao, Z. Liu, E. Adeli, and K. M. Pohl, "Longitudinal self-supervised learning," *Medical Image Analysis*, vol. 71, p. 102051, 2021.
- [182] D. Jung, J. Lee, J. Yi, and S. Yoon, "iCaps: An interpretable classifier via disentangled capsule networks," *arXiv:2008.08756*, 2020.
- [183] C. Qin, B. Shi, R. Liao, T. Mansi, D. Rueckert, and A. Kamen, "Unsupervised deformable registration for multi-modal images via disentangled representations," in *Proc. International Conference on Information Processing in Medical Imaging (IPMI)*, 2019, pp. 249–261.
- [184] S. Bakas, H. Akbari, A. Sotiras, M. Bilello, M. Rozycki, J. S. Kirby, J. B. Freymann, K. Farahani, and C. Davatzikos, "Advancing the cancer genome atlas glioma MRI collections with expert segmentation labels and radiomic features," *Scientific data*, vol. 4, no. 1, pp. 1–13, 2017.
- [185] K. He, H. Fan, Y. Wu, S. Xie, and R. Girshick, "Momentum contrast for unsupervised visual representation learning," in *Proc. IEEE/CVF Conference on Computer Vision and Pattern Recognition (CVPR)*, 2020, pp. 9726–9735.
- [186] T. Chen, S. Kornblith, M. Norouzi, and G. Hinton, "A simple framework for contrastive learning of visual representations," in *Proc. International Conference on Machine Learning (ICML)*, 2020, pp. 1597–1607.
- [187] T. Chen, S. Kornblith, K. Swersky, M. Norouzi, and G. E. Hinton, "Big self-supervised models are strong semi-supervised learners," in *Proc. International Conference on Neural Information Processing Systems (NeurIPS)*, 2020, pp. 22 243–22 255.
- [188] J.-B. Grill *et al.*, "Bootstrap your own latent: A new approach to self-supervised learning," *arXiv:2006.07733*, 2020.
- [189] J. Zbontar, L. Jing, I. Misra, Y. LeCun, and S. Deny, "Barlow twins: Self-supervised learning via redundancy reduction," *arXiv:2103.03230*, 2021.
- [190] J. Mitrovic, B. McWilliams, J. C. Walker, L. H. Buesing, and C. Blundell, "Representation learning via invariant causal mechanisms," *International Conference on Learning Representations (ICLR)*, 2021.
- [191] J. von Kugelgen, Y. Sharma, L. Gresele, W. Brendel,

- B. Schölkopf, M. Besserve, and F. Locatello, "Self-supervised learning with data augmentations provably isolates content from style," *arXiv:2106.04619*, 2021.
- [192] D. Li, Y. Yang, Y.-Z. Song, and T. M. Hospedales, "Learning to generalize: Meta-learning for domain generalization," in *Proc. AAAI Conference on Artificial Intelligence (AAAI)*, 2018.
- [193] M. L. Montero, C. J. Ludwig, R. P. Costa, G. Malhotra, and J. Bowers, "The role of disentanglement in generalisation," *International Conference on Learning Representations (ICLR)*, 2020.
- [194] R. Suter, D. Miladinovic, B. Schölkopf, and S. Bauer, "Robustly disentangled causal mechanisms: Validating deep representations for interventional robustness," in *Proc. International Conference on Machine Learning (ICML)*, 2019, pp. 6056–6065.
- [195] A. Stone, H. Wang, M. Stark, Y. Liu, D. Scott Phoenix, and D. George, "Teaching compositionality to CNNs," in *Proc. IEEE/CVF Conference on Computer Vision and Pattern Recognition (CVPR)*, 2017, pp. 5058–5067.
- [196] C. Marx, R. Phillips, S. Friedler, C. Scheidegger, and S. Venkatasubramanian, "Disentangling influence: Using disentangled representations to audit model predictions," in *Proc. International Conference on Neural Information Processing Systems (NeurIPS)*, 2019, pp. 4496–4506.
- [197] R. Aloufi, H. Haddadi, and D. Boyle, "Privacy-preserving voice analysis via disentangled representations," in *Proc. ACM SIGSAC Conference on Cloud Computing Security Workshop*, 2020, p. 1–14.
- [198] M. Jegorova, C. Kaul, C. Mayor, A. Q. O'Neil, A. Weir, R. Murray-Smith, and S. A. Tsafaris, "Survey: Leakage and privacy at inference time," *arXiv preprint arXiv:2107.01614*, 2021.
- [199] C. Dwork, "Differential privacy," in *International Colloquium on Automata, Languages, and Programming*. Springer, 2006, pp. 1–12.
- [200] N. Rieke *et al.*, "The future of digital health with federated learning," *NPJ Digital Medicine*, vol. 3, no. 1, pp. 1–7, 2020.